The Effect of Forced and Unforced Variability on Heat Waves, Temperature Extremes, and Associated Population Risk in a CO2-Warmed World

Jangho Lee[1], Jeffrey C. Mast[2], and Andrew E. Dessler[1]

[1]Texas A&M University
[2]Texas A&M

November 24, 2022

Abstract

This study investigates the impact of global warming heat and humidity extremes by analyzing 6-hourly output from 28 members of the Max Planck Institute Grand Ensemble driven by forcing from a 1%/year CO_2 increase. We find that unforced variability drives large changes in regional exposure to extremes in different ensemble members, and these variations are mostly associated with ENSO variability. However, while the unforced variability of the climate can alter the occurrence of extremes regionally, variability within the ensemble decreases significantly as one looks at larger regions or at a global population perspective. This means that, for metrics of extreme heat and humidity analyzed here, forced variability of the climate is more important than the unforced variability at global scales. Lastly, we found that most heat wave metrics will increase significantly between 1.5°C and 2.0°C, and that low GDP regions shows significant higher risks of facing extreme heat events compared to high GDP regions. Considering the limited economic adaptability of population on heat extremes, this reinforces the idea that the most severe impacts of climate change may fall mostly on those least capable to adapt.

The Effect of Forced and Unforced Variability on Heat Waves, Temperature Extremes, and Associated Population Risk in a CO_2-Warmed World

Jangho Lee, Jeffrey C. Mast, and Andrew E. Dessler

Department of Atmospheric Sciences, Texas A&M University, College Station, TX, USA

Corresponding author: Andrew Dessler (adessler@tamu.edu)

Key Points

- Unforced variability of the climate system, primarily ENSO, plays a key role in the occurrence of extreme events.

- Uncertainty of internal variability is shown to reduce as one looks at larger regions or at a global perspective by using the large Ensembles.

- Increases of heat wave indices are significant between 1.5°C and 2.0°C of warming and the risk of facing extreme heat events are higher in low GDP regions.

25   **Abstract**

26   This study investigates the impact of global warming heat and humidity extremes by

27   analyzing 6-hourly output from 28 members of the Max Planck Institute Grand Ensemble driven

28   by forcing from a 1%/year CO_2 increase. We find that unforced variability drives large changes

29   in regional exposure to extremes in different ensemble members, and these variations are mostly

30   associated with ENSO variability. However, while the unforced variability of the climate can

31   alter the occurrence of extremes regionally, variability within the ensemble decreases

32   significantly as one looks at larger regions or at a global population perspective. This means that,

33   for metrics of extreme heat and humidity analyzed here, forced variability of the climate is more

34   important than the unforced variability at global scales. Lastly, we found that most heat wave

35   metrics will increase significantly between 1.5°C and 2.0°C, and that low GDP regions shows

36   significant higher risks of facing extreme heat events compared to high GDP regions.

37   Considering the limited economic adaptability of population on heat extremes, this reinforces the

38   idea that the most severe impacts of climate change may fall mostly on those least capable to

39   adapt.

1. Introduction

The long-term goal of the 2015 Paris agreement is to keep the increase in global temperature well below 2°C above pre-industrial levels, while pursuing efforts and to limit the warming to 1.5°C. Given that no one lives in the global average, however, understanding how these global average thresholds translate into regional occurrences of extreme heat and humidity is of great value. Various studies have reported that regional extreme heat events and heat waves will not only be more frequent, but also more extreme in a warmer world. This was discussed in various assessment and reports such as US National Climate assessment and IPCC (Hoegh-Guldberg et al., 2018; Masson-Delmotte et al., 2018; Melillo et al., 2014; Wuebbles et al., 2017) and it is reported to have significant impacts on human society and health.

Many criteria and indices have been used to assess extreme heat, such as the absolute increase of maximum temperature from the reference period (Wobus et al., 2018), risk ratio (Kharin et al., 2018), and heat wave magnitude index (Russo et al., 2017). In this study, we utilize four locally defined heat wave indices from Fischer (2010) and Perkins (2012), of duration, frequency, amplitude, and mean. We also focus on consecutive-day extremes, which are known to cause more harm than single-day events (Baldwin et al., 2019; Simolo et al., 2011; Tan et al., 2010). In addition, because the combined effect of temperature and humidity is known to affect human health by reducing the body's ability to cool itself through perspiration, wet-bulb temperature is frequently analyzed (Kang & Eltahir, 2018) and we will do so here.

Climate extremes are always a combination of long-term forced climate change acting in concert with unforced variability (Deser et al., 2012). Thus, characterizing and quantifying the variability of the climate system is crucial in assessing the future risk of extreme events. There have been numerous studies that links dominant modes of unforced variability to extreme events.

63 Temperature connections with El Niño Southern Oscillation (ENSO) (Meehl et al., 2007;

64 Thirumalai et al., 2017), Pacific Decadal Oscillation (PDO) (Birk et al., 2010) , Atlantic

65 Multidecadal Oscillation (AMO) (Zhang et al., 2020) have been investigated from the previous

66 studies. The effect of climate extremes on different populations depends on the level of

67 economic development, with impacts of heat extremes being more severe in less economically

68 developed countries (Diffenbaugh & Burke, 2019; Harrington et al., 2016; King & Harrington,

69 2018). For example, as temperatures go up, increased energy demand to cool buildings will be

70 required (Parkes et al., 2019; Sivak, 2009). But this requires resources to both install air

71 conditioning and then run it.

72   In this paper, a single-model initial-condition ensemble of 28 runs of a global climate

73 model (GCM) is used to quantify heat and humidity extremes in a warmer world. We use

74 population data to look at population risk as well as thresholds for mortality events in daytime

75 (Mora et al., 2017) and nighttime (Chen & Lu, 2014). We also utilize GDP per capita data to

76 investigate how climate change impacts different levels of economic status during extreme

77 events. To quantify the impact on energy demand, we also quantify changes in cooling degree

78 days and warming degree days.

79   The rest of the paper will focus on the following topics: Section 2 describes the model

80 and data used, Section 3 explains the bias-correction method, as well as explaining the metrics

81 used. Section 4 describes the results of the calculations and associated heat wave events in the

82 warmer world as well as the role of unforced variability on extreme heat events. Section 5

83 summarizes the results and suggests directions for the future work.

84

85 **2. Data**

86   *2.1. MPI-ESM 1% CO$_2$ runs*

87   Simulation data in this study come from an ensemble of runs of the Max-Plank Institute

88   Earth System Model collectively known as the MPI Grand Ensemble (MPI-GE) project (Maher

89   et al., 2019). Each of the 28 ensemble members branches from different points of a 2000-year

90   pre-industrial control run and go for 150 years, forced by CO$_2$ concentration increasing at 1% per

91   year (hereafter, 1% runs). Because forcing scales as the log of CO$_2$ concentration, the 1% runs

92   feature radiative forcing that increases approximately linearly in time. We analyze 6-hourly

93   output with 1.875° × 1.875° spatial resolution for land and near-land ocean areas between 60°N

94   and 60°S. Our analysis will focus on 2-meter temperature (hereafter, t2m) and 2-meter dew point

95   temperature (d2m), from which 2-meter relative humidity and wet-bulb temperature (w2m) are

96   calculated using the equations of Stull (2011).

97   Unforced variability in the climate system generates uncertainties in the projection of the

98   climate by impacting the dynamic component of the climate, especially for extreme events (Kay

99   et al., 2015; Thompson et al., 2015). In this paper, we use the ensemble to allow us to estimate

100   the impact of unforced variability on temperature extremes.

101   We also analyze a 100-member ensemble of runs of the same model with historical

102   forcing (hereafter, historical runs), which is also a subset of MPI-GE. Each of the 100 members

103   simulates the years 1850-2005 and uses identical historical natural and anthropogenic forcing.

104   Like the 1% runs, each historical ensemble member branches from a different point in the same

105   2000-year control run. This historical ensemble only has monthly average fields.

106

107   *2.2. Global population and GDP per capita data*

108   Global population data from the NASA Socioeconomic Data and Applications Center

109   (SEDAC, 2018) are used to weight the heat wave indices by population. The data represent the

110   population in year 2015 at $30'' \times 30''$ spatial resolution, and we averaged and re-gridded to the

111    $1.875° \times 1.875°$ grid of the MPI model by summing the values in grid boxes surrounding the

112   MPI grid centers. In our population-weighted calculations, we assume that the relative

113   distribution of population remains fixed into the future.

114   Gridded GDP per capita data (Kummu, 2019) over 1990-2015 are used to estimate the

115   risk of heat extreme events for different levels of wealth. These data are regridded from the

116   original $5'' \times 5''$ spatial resolution to the MPI model's resolution of $1.875° \times 1.875°$ by

117   averaging the GDP inside the grid box. When averaging the GDP, per capita GDP has been

118   multiplied by population to estimate the total GDP. Data were then averaged over the 1990-2015

119   period. We assume that the relative percentile of GDP per capita for each grid point is assumed

120   to be fixed into the future, so changes in climate risk are due to exposure to warmer climate

121   extremes, not changes in relative per capita wealth.

122

123   **3. Method of analysis**

124   *3.1. Global warming*

125   Global warming is defined as the global and annual average temperature increase

126   compared to the first 5 years of the 1% run. We find that ensemble- and global-average t2m

127   reaches 1.5°C, 2°C, and 4°C occur in years 59, 76, and 133 years, respectively, and reaches

128   4.59°C at the end of the 150-year run. The increase of global average temperature is nearly linear

129   for both t2m and w2m (Figure 1a and 1b), consistent with a linear ramping of the forcing.

130

131   *3.2. Bias-correction of 1% runs*

132   Many GCMs have systematic biases in surface temperature, and various attempts have

133   been made to correct them (e.g. Li et al., 2010; Thrasher et al., 2012). In our analysis, we are

134   mainly interested in the spatial pattern of warming, and to judge the fidelity of that in the MPI-

135   ESM 1.1 model, we compare the 1% runs with ERA-Interim reanalysis data (Dee et al., 2011)

136   from European Centre for Medium-range Weather Forecast (ECMWF). To do this, we compared

137   the period 2003-2017 in the ERA-interim with a 15-year period in the 1% runs (years 39-53)

138   with the same ensemble- and global-average absolute temperature. The ensemble and area-

139   averaged bias for land and near-land ocean areas archived in the 6-hourly dataset is near zero for

140   t2m, but underestimates w2m over this period by 0.18°C (Figure 1).

141   But while the ensemble- and area-averaged t2m bias is near zero, the difference is not

142   zero at all grid points of individual ensemble members. Figures 2a and 2b show the difference in

143   the 90th percentile value of t2m and w2m at each grid point calculated over the 15-year period in

144   the model ensemble minus the 90th percentile value at the same grid point in the ERA-Interim.

145   Figures 2c and 2d show the difference in median values.

146   This bias is not the result of unforced variability — it is consistent in all ensemble

147   members. To show this, we calculate at each grid point the difference between the highest and

148   lowest 90th percentile temperature in the ensemble divided by the ensemble average 90th

149   percentile temperature bias between reanalysis data the ensemble, computed where the bias is

150   greater than 2°C (Figure 2e). We also do the same for the median temperature (Figure 2f). The

151   disagreement between the ensembles is at most 37% of the bias in the same region, and the

152   average is 13% (Figures 2e, f). In other words, the systematic bias of the model compared to

153   reanalysis exceeds the spread within the ensemble.

154   The CDF-t method (Michelangeli et al., 2009) is used to bias correct the 1% runs. CDF-t

155   method finds the transformation function that maps the cumulative density function (CDF) of a

156   GCM to the CDF of a historical reanalysis data in a reference period, which is year 39-53 in 1%

157   runs and 2003-2017 for ERA-Interim reanalysis data. This function is then applied to the 1%

158   runs to generate bias-corrected fields. For the values that fall outside the limits of the CDFs in

159   the reference period, linear extrapolation is used. CDF-t is known to realistically correct the

160   temperature and precipitation output of GCMs, especially for extreme events (Vrac et al., 2012;

161   Watanabe et al., 2012).

162   Bias correction via CDF-t is done for t2m and d2m, and then rh and w2m are calculated

163   with these bias-corrected fields. The bias is reduced significantly for all regions for both t2m and

164   w2m (Figures 1c, 1d, 2a-2d). The bias in w2m is mostly caused by the small remaining biases in

165   t2m and d2m, which are amplified in the w2m calculation. Hereafter, '1% runs' will refer to the

166   bias-corrected 1% runs.

167   Since the 1% runs are CO_2-only forcing, without aerosol forcing, one might wonder

168   whether the temperature extremes estimated by these models would apply to a world with a more

169   realistic forcing that includes aerosols. To determine this, we have compared monthly average

170   and monthly maximum temperatures from an ensemble of 100 RCP 8.5 scenario runs from the

171   MPI-GE to the same quantities estimated from the 1% ensemble. If we compare the ensembles

172   at points in time when they have 1.5, 2, 3, and 4°C of ensemble- and global-average warming,

173   we find very small regional differences — the regional ensemble averaged maximum and mean

174   temperature difference was less than 0.5°C in all regions. Alternatively, since we bias-corrected

175   the 1% CO_2 runs to reanalysis data, which contains aerosol forcing, our bias-corrected 1% CO_2

176   runs can be understood as a continuously warming climate driven by CO_2, with effect of aerosols

177   fixed at 2003-2017 period.

178

179   *3.3. Heat wave indices*

180   Identification of heat waves is done in several steps. First, we smooth a daily maximum

181   temperature (determined form 6-hourly temperatures) using a 15-day moving window for the

182   first 5 years of 1% runs, which is the period before significant warming has occurred. This was

183   done at each grid points, followed by a framework from Fischer (2010). Then, also for each grid

184   point, the 90th percentile of smoothed daily maximum temperature for the first 5 years was

185   calculated. This value is used as a threshold for the heat waves. After calculating the threshold,

186   we calculate the heat wave days, defined as days that exceeds the threshold for three or more

187   consecutive days (Baldwin et al., 2019).

188   We then define four indices to represent the characteristics of these heat waves. To

189   determine the occurrence of events, heat wave duration (HWD; longest heat wave of the year)

190   and heat wave frequency (HWF; total number of heat wave days in a year) are calculated. From

191   an intensity perspective, heat wave amplitude (HWA; maximum temperature during heat wave

192   days during a year) and heat wave mean (HWM; mean temperature during heat wave days in a

193   year) are selected. These indices are also calculated in an analogous fashion for wet bulb

194   temperature (w2m), since wet-bulb temperature is arguably more relevant for human health

195   (Buzan & Huber, 2020; Heo et al., 2019; Morris et al., 2019). These indices are summarized in

196   Table l.

197

198   *3.4. Deadly days and tropical nights*

199   Heat wave thresholds are different for each grid point because they are based on pre-

200   industrial baseline at that grid point. Combined with regional differences in the ability to adapt,

201   this means that heat waves in different regions may have different implications for human

202   society. We therefore also count the number of days each year with w2m above 24°C, which we

203   refer to as "deadly days". This value is consistent with the analysis of Mora et al., (2017), who

204   demonstrated that this is the threshold above which fatalities from heat-related illness occur. A

205   warm nighttime minimum temperature can be as important as a high maximum temperature for

206   human health and mortality (Argaud et al., 2007; Patz et al., 2005), so we define "tropical nights"

207   as a daily minimum t2m over 25°C (Lelieveld et al., 2012).

208

209   *3.5. Cooling degree days and heating degree days*

210   To assess the economic and energy impact of heat extremes, cooling degree days (CDD)

211   and heating degree days (HDD) are calculated. CDD and HDD are metrics of the energy demand

212   to cool and heat buildings. For each grid point, annual CDD is calculated by subtracting 18°C

213   from the daily average temperature and summing only the positive values over the year. HDD is

214   the absolute value of the sum of the negative values. Although energy demand could be highly

215   linked to the culture, wealth, population of the region and other meteorological conditions rather

216   than the daily mean temperature, previous studies reported that CDD and HDD are closely

217   related to energy consumption (Sailor & Muñoz, 1997).

218

219   **4. Results**

220   *4.1. Impact of unforced variability of climate on regional heat extremes*

221   To investigate the impact of unforced variability on more regional heat extremes, we

222   select 15 large cities spread around the world (Fig. 3a). Figure 3b-d shows the maximum spread

223   in the number of deadly days and tropical nights within the ensemble — i.e., the difference

224   between the ensemble member with the highest values of extreme events (deadly days, tropical

225   nights) minus the member with the lowest — at a year when ensemble- and global-average

226   temperature reaches the threshold.

227   This difference within the ensemble is the result of unforced variability and we see that it

228   varies considerably among the cities. For example, Moscow shows a small spread within the

229   ensemble for both deadly days and tropical nights for all periods of global warming. This is

230   because, even with 4°C of warming, Moscow experiences a maximum of only 8 deadly days and

231   25 tropical nights per year. In contrast, with 3°C of warming, a warmer city such as Kinshasa

232   experiences 148 more deadly days in some ensembles than others, and 55 more tropical nights.

233   For all 15 cities, average spread in the number of deadly days at 1.5°C, 2.0°C, 3.0°C , and 4.0°C

234   of global warming between the ensemble members with maximum and minimum numbers is

235   53.5, 53.2, 63.6, and 56.8 days per year. For tropical nights, the spread is 50.4, 50.3, 50.9, and

236   52.2 days per year. So, on average, unforced variability can change the number of extreme days

237   and nights by about two months per year.

238   Previous work has attempted to distinguish the origin and mechanisms of unforced

239   variability from temperature and temperature extremes (Birk et al., 2010; Meehl et al., 2007;

240   Zhang et al., 2020). To probe the physical mechanisms affecting this spread of ensembles,

241   empirical orthogonal function (EOF) analysis was performed separately on the detrended and

242   normalized time series of deadly days and tropical nights for the 15 cities across the ensemble.

243   We aim to find the dominant drivers of unforced variability that impacts representative cities

244   around the world.

245   The first three EOF patterns are plotted in Fig. 4. The first EOF mode of deadly days per

246   year in 15 cities show similar signs for all cities except Istanbul and Kinshasa, where the

247   magnitude of the EOF is small for both cities. This means that, if one of the cities is hot, then the

248   others also tend to be hot. The second and third EOFs for deadly days shows more variability

249   between the cities. The EOFs for tropical nights (Fig. 4d, 4e, 4f) shows more variability, with

250   higher frequency of tropical nights in some cities associated with lower values in others.

251   The PC time series are projected onto detrended annual sea surface temperature (SST)

252   anomalies, and this is also plotted in Fig. 4. All of the projections of deadly day PCs and

253   projections of the first two modes of tropical nights shows patterns similar to El Niño-Southern

254   Oscillation (ENSO) and Pacific Decadal Oscillation (PDO). Characteristic patterns for ENSO,

255   PDO, and AMO are calculated for each ensemble using all 150-year of SSTs, and the pattern is

256   averaged over ensembles to come up with a single ENSO, PDO, and AMO SST for the ensemble.

257   Then, those patterns are compared with the PC projection on SST. Correlation coefficients

258   between the standard climate indices and PC projected SST is shown on lower panel of Fig. 4.

259   Power spectra of the PCs are plotted in Figure 5. Overall, the spectra of the deadly day

260   PCs look very much like the spectrum for ENSO, but does not have the ~20-year peak of the

261   PDO spectrum. This tells us that, in this model at least, the variability in the occurrence of

262   deadly days in these large cities is strongly regulated by ENSO. The third deadly day PC has

263   lower correlations with ENSO or PDO index and a peak at both the ENSO period a slightly

264   longer period than ENSO, about 10 years, so it is harder to draw firm conclusions about the

265   mechanism behind it.

266   The tropical night PCs also show peaks at ENSO periods (Fig. 5b) suggesting that, like

267   deadly days, tropical night variability is controlled by ENSO. However, the PC-projected SST

268   of the third EOF of tropical nights shows high values near Northern Africa and East Asian region,

269   suggesting that this EOF represents the effect of ENSO on tropical night variability in this region.

270

271   *4.2. Cluster analysis and population risk of heat wave indices*

272   We calculate HWD, HWF, HWA, and HWM for both t2m and w2m each year at each

273   grid point, which generates eight different 150-year time series for each of the 28 ensemble

274   members. Each time series at each grid point is regressed vs. time, yielding a slope and the

275   intercept for each time series in all of the 28 ensemble members. The 16 variables (8 [heat wave

276   indices] × 2 [slope, intercept]) are then utilized as a predictor variable for K-means clustering

277   (Likas et al., 2003) to categorize the spatial variation of heat waves. K-means clustering aims to

278   classify the observations (grid point over land) into clusters using the Euclidean distance of its

279   predictor variables (16 variables). The number of clusters (K) in this study is set to 6, using the

280   elbow method (Syakur et al., 2018).

281   Figure 6a shows the cluster value that most ensembles assigned to each grid point and it

282   shows distinct geographical characteristics, as summarized in Table 2 (the result of clustering

283   shows little difference between the ensemble members). As might be expected, each cluster

284   shows a different evolution of heat extremes in warmer world (Figure 7). Although the warming

285   signal is largest in the polar regions (Figure 6b), the largest increases of HWD and HWF are

286   observed at lower latitudes (in cluster 1 and 2 on Figure 7a-d). This is due to low variability in

287   these regions compared to polar regions, making it easier for a trend to exceed the heatwave

288   threshold.

289   For HWA and HWM, the rate of increase is similar for all clusters, with increases of

290 HWA_{t2m} and HWA_{w2m} of 3.5 and 2.2°C, respectively (Figure 7e-h). The exception is HWA_{t2m} in

291 cluster 6. The large increase of HWA_{t2m} in this region is connected to the strong global warming

292 signal in high latitudes that has been predicted for decades and now observed (Stouffer &

293 Manabe, 2017).

294   Turning to deadly days (Fig. 7i), we find a substantial increase occurs in cluster 1 after

295 1.5°C of warming; this is important because it gives additional support for the Paris Agreement's

296 aspirational goal of limiting global warming to 1.5°C. Almost all of the increases in deadly days

297 are in low latitudes (cluster 1, 2, and 3). For tropical nights, low latitudes as well as deserts

298 (cluster 4) contribute most of the increase. These regions also show more rapid increases when

299 global average warming exceeds 1.5-2°C.

300   Figure 7 also shows the spread in within the ensemble for each metric and cluster. We

301 find that the spread for a cluster is generally smaller than the differences between the clusters.

302 This suggests that the differences obtained are not due to interannual variability.

303   We also generated indices weighted by population. Heat wave indices for the 90th

304 percentile of population (meaning 10% of the population is exposed to higher values) and

305 median of the population are depicted in Figure 8. Figure 8a shows that with 4°C of warming, 10%

306 of the Earth's population will experience heat waves lasting 131 days, and half of the population

307 will experience heat waves around 64 days long. These are large increases over present-day

308 values of 35 days and 17 days. Notably, the average of the standard deviation between the

309 ensembles during 150-yr period are 6.7 days and 3.4 days for the 90th percentile and median,

310 respectively. This is significantly smaller than values from the regional analyses of cities in

311   Figure 3, where the unforced variability can make a huge difference in the occurrence of heat

312   waves.

313   The rate of increase of HWD_{w2m} and HWF_{w2m} in Fig. 8 accelerates when global average

314   warming exceeds 1-1.5°C. Given that the planet has already warmed about 1°C above pre-

315   industrial, this suggests that the world may be on the cusp of a rapid increase in wet-bulb

316   extremes. This is related to the increased slope in Figure 7, in which cluster 1 and 2's values of

317   HWD_{w2m} and HWF_{w2m} increase rapidly between 1.5C and 2.5°C of global warming. At warmer

318   temperatures, HWD_{w2m} and HWF_{w2m} reach a plateau, since values over 300 days per year means

319   there is little room for additional increase. For $HWA_{t2m/w2m}$ and $HWM_{t2m/w2m}$, the increase is

320   mostly linear. Also note that at 4°C of global warming, HWA_{w2m} reaches 30°C, which while not

321   immediately fatal to humans may nevertheless indicate great difficulty for even a developed

322   society to adapt to.

323   Currently, 5% of the total population faces more than 180 deadly days and 302 tropical

324   nights per year. This grows to 204 and 333 days, respectively, at 1.5°C warming. With 2°C of

325   global warming, half of the population will face 2 months of deadly days every year and with

326   2.5°C of global warming, and 5% of the population will be in an environment where every day in

327   a year is a tropical night. With 2°C of global warming, the minimum ensemble member of

328   deadly days and tropical nights is above the maximum ensemble of the current climate. Further

329   details are also shown in Table 3.

330   It is notable that, although there is a large spread between the ensemble members in each

331   city (Figure 3), the spread in the clusters (Figure 7) and population-weighted metrics (Figure 8)

332   is not as large. This emphasizes that the effect of unforced variability might be large in small

333   regions, but as the region expands, opposite signs of variability cancel, so area-average

334   variability decreases. This is also found in Table 3, where in each case, the standard deviation

335   between ensembles is less than 10% of the average. This indicates that natural variability will

336   play a minor role in determining global exposure to temperature thresholds, although different

337   people may be affected in different climate realizations.

338   In addition, with 1.5°C of global warming, the lowest ensemble of the 90th percentile of

339   HWD_{t2m}, HWD_{w2m}, and HWF_{t2m} exceeds the highest ensemble of the same metric in the current

340   climate (red lines in Figure 8). With 2°C of warming, the minimum ensemble of HWF_{w2m},

341   HWA_{t2m}, HWA_{w2m}, and HWM_{w2m} exceed the maximum ensemble of the current climate, and

342   with 2.5°C of warming, the minimum ensemble of all metrics exceeds the maximum ensemble of

343   the same metric in the current climate. Thus, this model predicts that the occurrence of extremes

344   will soon be able to exceed values likely possible in our present climate.

345

346   *4.3. Analysis on GDP per capita*

347   It is well-known that not everyone is equally vulnerable to extreme weather, with rich,

348   developed countries having more resources to deal with extreme events. In that context, global

349   gridded GDP per capita is used to calculate average risk at each level of wealth. The ensemble-

350   average result is depicted in Figure 9, which shows the increased number of deadly days and

351   tropical nights that each level of economic level experience relative to today's current level of

352   global warming. This plot assumes that the distribution of population and GDP remains fixed

353   through time.

354   With 0.5°C increase of global warming, population in lowest 10% of GDP will face 28

355   more deadly days and 22 more tropical nights increasing compared to present day. In contrast,

356   the richest 10% will experience 5 and 3 more deadly days and tropical nights for the same

357   warming. At 3°C above current temperatures (about 4°C above preindustrial temperatures), the

358   population with the lowest 10% of GDP will experience154 and 162 more days of deadly days

359   and tropical nights compared to today's climate. On the other hand, population with the highest

360   10% of GDP will experience an increase of 26 and 30 days for the same warming. The regions

361   that contribute the most for the low GDP percentiles are Tropical Africa, including Republic of

362   the Congo, Kenya, Uganda, Ethiopia, and Sudan, which are in clusters 1 and 2 in our cluster

363   analysis. The maximum difference of heat wave days between the ensembles is less than 25% for

364   all GDP and global warming levels.

365

366   *4.4. Energy demand on large cities*

367   Annual CDD and HDD have been calculated for the 15 cities in section 4.1. Fig. 10

368   shows the percent change of CDD and HDD at 1.5°C, 2.0°C, 3.0°C, and 4.0°C relative to the

369   pre-industrial CDD and HDD values (average of first 5 year of 1% CO_2 runs). This was done for

370   each city, and for each ensemble member. In 1.5°C, 2.0°C, 3.0°C, and 4.0°C warming, CDD in

371   15 cities increases by 26%, 38%, 60%, and 82%. This suggests an enormous increase in energy

372   required for cooling. In contrast, energy demand on cold days (HDD) decreases by 51%, 60%,

373   68%, and 75%, compared to pre-industrial baseline, suggesting a partially offsetting decrease in

374   energy required for heating. The spread between the ensemble members is small compared to the

375   average of the ensembles, except for Moscow.

376   Large percentage increases in CDD for Moscow is the result of low pre-industrial CDD

377   values, so that (relatively) small increases in CDD correspond to large fractional changes, as well

378   as large differences between ensemble members. The ensemble spread of HDD in Moscow is

379   also large, compared to other cities. This is not due to low values of HDD – Moscow has highest

380 HDD value among 15 cities (4062 days °C per year in pre-industrial condition) — but rather that

381 unforced variability of the climate is more important for HDD than CDD values for Moscow.

382

383 **5. Conclusion**

384   In this study, we found that extreme heat events will become more frequent and severe in

385 a continuously warming world. In a warmer world, duration, frequency, amplitude, and mean of

386 extreme heat and humidity events increase, especially in low-latitude regions. In some of the

387 regions, wet bulb temperature will reach upper 20s, which is above the level that significantly

388 impact human mortality. We also find and quantify the impact of forced change and unforced

389 variability on the extreme heat events.

390   Our results show that ENSO is the dominant mode of unforced variability impacting the

391 occurrence of extreme heat and humidity events and that events tend to be synchronous in 15

392 large cities we chose. But while the impact of unforced variability might be significant regionally,

393 it narrows down when one looks at larger aggregate regions.

394   Looking at the population-weighted stats, we found that with 1.5°C of global average

395 warming, over 10% of population will face heat waves of 42°C temperature, and 27°C wet bulb

396 temperatures. With 4°C warming, 10% of population will face 45°C temperature and 29°C wet

397 bulb temperature. Also, even with 1.5°C of warming, which is about 0.5°C higher than the

398 current level, 5% of the population will face more than 200 days of deadly days and over 300

399 days of tropical nights per year. With 4°C of warming, 10% of the population will experience

400 over 300 days of deadly days and over 330 days of tropical nights per year. Given these two

401 metrics are based on human mortality, this may have significant impact on human health

402 globally.

403   Sorting heat and humidity events by wealth, we found that increasing frequency and

404   severity of extreme events will fall mostly on the poorest people. Given underdeveloped

405   countries' lack of ability to endure climate extremes, and that they have contributed the least to

406   climate change, this introduces a profound moral dimension to the problem. To further

407   investigate the economic impacts of increasing heat extremes, cooling degree days (CDD) and

408   heating degree days (HDD) are calculated for 15 large cities. Energy demand for cooling (CDD)

409   increases by average of 26% on 1.5°C and 82% on 4.0°C of warming, while energy demand for

410   heating (HDD) decreases by 51% and 75%. Since CDD is known to have a conditionally linear

411   relationship with the energy consumption, with slope increasing with higher CDD (De Rosa et al.,

412   2014; Shin & Do, 2016), increasing CDD in a warmer world could be one of the factors driving

413   increased economic inequity from global warming related heat extremes, due to high cost and

414   demand for energy in poorest countries.

415   Uncertainties in this analysis include our use of gridded 6-hourly climate model output.

416   Another uncertainty is that our runs are continuously warming, and it is possible that an

417   equilibrium world at any given temperature may experience different occurrence of extremes

418   than in the runs in this paper. Additionally, since an increasing proportion of the population lives

419   in dense metropolitan areas, there is also the possibility that actual heat and humidity extremes

420   that populations experience could be more severe than the gridded data due to local phenomena

421   such as the urban heat island effect (Murata et al., 2012). Statistical or dynamical downscaling

422   could be used for a more detailed analysis (Dibike & Coulibaly, 2006; Wood et al., 2004). This

423   was not done in this study because the model we used is already bias-corrected, so another

424   downscaling would affect the consistency of the model. However, better understanding and

425   evaluation of the actual temperatures people are projected to experience would be a useful next

426   step.

427

428   **Acknowledgments**

References

Argaud, L., Ferry, T., Le, Q. H., Marfisi, A., Ciorba, D., Achache, P., et al. (2007). Short- and long-term outcomes of heatstroke following the 2003 heat wave in Lyon, France. *Archives of Internal Medicine, 167*(20), 2177-2183. <Go to ISI>://WOS:000250806200003

Baldwin, J. W., Dessy, J. B., Vecchi, G. A., & Oppenheimer, M. (2019). Temporally Compound Heat Wave Events and Global Warming: An Emerging Hazard. *Earths Future, 7*(4), 411-427. <Go to ISI>://WOS:000467396900007

Birk, K., Lupo, A. R., Guinan, P., & Barbieri, C. (2010). The interannual variability of midwestern temperatures and precipitation as related to the ENSO and PDO. *Atmosfera, 23*(2), 95-128.

Buzan, J. R., & Huber, M. (2020). Moist heat stress on a hotter Earth. *Annual Review of Earth and Planetary Sciences, 48*.

Chen, R. D., & Lu, R. Y. (2014). Dry Tropical Nights and Wet Extreme Heat in Beijing: Atypical Configurations between High Temperature and Humidity. *Monthly Weather Review, 142*(5), 1792-1802. <Go to ISI>://WOS:000335115400006

De Rosa, M., Bianco, V., Scarpa, F., & Tagliafico, L. A. (2014). Heating and cooling building energy demand evaluation; a simplified model and a modified degree days approach. *Applied energy, 128*, 217-229.

Dee, D. P., Uppala, S. M., Simmons, A. J., Berrisford, P., Poli, P., Kobayashi, S., et al. (2011). The ERA-Interim reanalysis: configuration and performance of the data assimilation system. *Quarterly Journal of the Royal Meteorological Society, 137*(656), 553-597. <Go to ISI>://WOS:000290450900001

Deser, C., Phillips, A., Bourdette, V., & Teng, H. Y. (2012). Uncertainty in climate change projections: the role of internal variability. *Climate Dynamics, 38*(3-4), 527-546. <Go to ISI>://WOS:000299899300006

Dibike, Y. B., & Coulibaly, P. (2006). Temporal neural networks for downscaling climate variability and extremes. *Neural Networks, 19*(2), 135-144. <Go to ISI>://WOS:000237527600004

Diffenbaugh, N. S., & Burke, M. (2019). Global warming has increased global economic inequality. *Proceedings of the National Academy of Sciences, 116*(20), 9808-9813.

Fischer, E. M., & Schär, C. (2010). Consistent geographical patterns of changes in high-impact European heatwaves. *Nature Geoscience, 3*(6), 398-403.

Harrington, L. J., Frame, D. J., Fischer, E. M., Hawkins, E., Joshi, M., & Jones, C. D. (2016). Poorest countries experience earlier anthropogenic emergence of daily temperature extremes. *Environmental Research Letters, 11*(5), 055007.

Heo, S., Bell, M. L., & Lee, J. T. (2019). Comparison of health risks by heat wave definition: Applicability of wet-bulb globe temperature for heat wave criteria. *Environmental Research, 168*, 158-170. <Go to ISI>://WOS:000452938700019

Hoegh-Guldberg, O., Jacob, D., Bindi, M., Brown, S., Camilloni, I., Diedhiou, A., et al. (2018). Impacts of 1.5 C global warming on natural and human systems. *Global warming of 1.5° C. An IPCC Special Report*.

Kang, S., & Eltahir, E. A. B. (2018). North China Plain threatened by deadly heatwaves due to climate change and irrigation. *Nat Commun, 9*(1), 2894. https://www.ncbi.nlm.nih.gov/pubmed/30065269

476 Kay, J. E., Deser, C., Phillips, A., Mai, A., Hannay, C., Strand, G., et al. (2015). THE COMMUNITY
477   EARTH SYSTEM MODEL (CESM) LARGE ENSEMBLE PROJECT A Community Resource for
478   Studying Climate Change in the Presence of Internal Climate Variability. *Bulletin of the*
479   *American Meteorological Society, 96*(8), 1333-1349. <Go to
480   ISI>://WOS:000361366100002
481 Kharin, V. V., Flato, G. M., Zhang, X., Gillett, N. P., Zwiers, F., & Anderson, K. J. (2018). Risks from
482   Climate Extremes Change Differently from 1.5 degrees C to 2.0 degrees C Depending on
483   Rarity. *Earths Future, 6*(5), 704-715. <Go to ISI>://WOS:000435639800003
484 King, A. D., & Harrington, L. J. (2018). The inequality of climate change from 1.5 to 2 C of global
485   warming. *Geophysical Research Letters, 45*(10), 5030-5033.
486 Kummu, M. T., Maija; Guillaume, Joseph H. A. (2019). *Data from: Gridded global datasets for*
487   *Gross Domestic Product and Human Development Index over 1990-2015 Dryad, Dataset,*
488   *https://doi.org/10.5061/dryad.dk1j0*.
489 Lelieveld, J., Hadjinicolaou, P., Kostopoulou, E., Chenoweth, J., El Maayar, M., Giannakopoulos,
490   C., et al. (2012). Climate change and impacts in the Eastern Mediterranean and the
491   Middle East. *Climatic Change, 114*(3-4), 667-687. <Go to ISI>://WOS:000308246300014
492 Li, H. B., Sheffield, J., & Wood, E. F. (2010). Bias correction of monthly precipitation and
493   temperature fields from Intergovernmental Panel on Climate Change AR4 models using
494   equidistant quantile matching. *Journal of Geophysical Research-Atmospheres, 115*. <Go
495   to ISI>://WOS:000277965100006
496 Likas, A., Vlassis, N., & Verbeek, J. J. (2003). The global k-means clustering algorithm. *Pattern*
497   *Recognition, 36*(2), 451-461. <Go to ISI>://WOS:000179225600015
498 Maher, N., Milinski, S., Suarez-Gutierrez, L., Botzet, M., Dobrynin, M., Kornblueh, L., et al.
499   (2019). The Max Planck Institute Grand Ensemble: Enabling the Exploration of Climate
500   System Variability. *Journal of Advances in Modeling Earth Systems, 11*(7), 2050-2069.
501   <Go to ISI>://WOS:000480282800010
502 Masson-Delmotte, V., Zhai, P., Pörtner, H.-O., Roberts, D., Skea, J., Shukla, P. R., et al. (2018).
503   Global warming of 1.5 C. *An IPCC Special Report on the impacts of global warming of, 1*.
504 Meehl, G. A., Tebaldi, C., Teng, H., & Peterson, T. C. (2007). Current and future US weather
505   extremes and El Niño. *Geophysical Research Letters, 34*(20).
506 Melillo, J. M., Richmond, T., & Yohe, G. (2014). Climate change impacts in the United States.
507   *Third national climate assessment, 52*.
508 Michelangeli, P. A., Vrac, M., & Loukos, H. (2009). Probabilistic downscaling approaches:
509   Application to wind cumulative distribution functions. *Geophysical Research Letters, 36*.
510   <Go to ISI>://WOS:000267000400001
511 Mora, C., Dousset, B., Caldwell, I. R., Powell, F. E., Geronimo, R. C., Bielecki, C. R., et al. (2017).
512   Global risk of deadly heat. *Nature Climate Change, 7*(7), 501-+. <Go to
513   ISI>://WOS:000404545400017
514 Morris, C. E., Gonzales, R. G., Hodgson, M. J., & Tustin, A. W. (2019). Actual and simulated
515   weather data to evaluate wet bulb globe temperature and heat index as alerts for
516   occupational heat-related illness. *Journal of Occupational and Environmental Hygiene,*
517   *16*(1), 54-65. <Go to ISI>://WOS:000471113200009

518 Murata, A., Nakano, M., Kanada, S., Kurihara, K., & Sasaki, H. (2012). Summertime temperature
519   extremes over Japan in the late 21st century projected by a high-resolution regional
520   climate model. *Journal of the Meteorological Society of Japan. Ser. II, 90*, 101-122.
521 Parkes, B., Cronin, J., Dessens, O., & Sultan, B. (2019). Climate change in Africa: costs of
522   mitigating heat stress. *Climatic Change, 154*(3-4), 461-476.
523 Patz, J. A., Campbell-Lendrum, D., Holloway, T., & Foley, J. A. (2005). Impact of regional climate
524   change on human health. *Nature, 438*(7066), 310-317. <Go to
525   ISI>://WOS:000233300200039
526 Perkins, S., Alexander, L., & Nairn, J. (2012). Increasing frequency, intensity and duration of
527   observed global heatwaves and warm spells. *Geophysical Research Letters, 39*(20).
528 Russo, S., Sillmann, J., & Sterl, A. (2017). Humid heat waves at different warming levels.
529   *Scientific Reports, 7*. <Go to ISI>://WOS:000407080100107
530 Sailor, D. J., & Muñoz, J. R. (1997). Sensitivity of electricity and natural gas consumption to
531   climate in the USA—Methodology and results for eight states. *Energy, 22*(10), 987-998.
532 SEDAC. (2018). *Gridded Population of the World, Version 4 (GPWv4): Population Density,
533   Revision 11*.
534 Shin, M., & Do, S. L. (2016). Prediction of cooling energy use in buildings using an enthalpy-
535   based cooling degree days method in a hot and humid climate. *Energy and Buildings,
536   110*, 57-70.
537 Simolo, C., Brunetti, M., Maugeri, M., & Nanni, T. (2011). Evolution of extreme temperatures in
538   a warming climate. *Geophysical Research Letters, 38*. <Go to
539   ISI>://WOS:000294129400005
540 Sivak, M. (2009). Potential energy demand for cooling in the 50 largest metropolitan areas of
541   the world: Implications for developing countries. *Energy Policy, 37*(4), 1382-1384.
542 Stouffer, R. J., & Manabe, S. (2017). Assessing temperature pattern projections made in 1989.
543   *Nature Climate Change, 7*(3), 163-165.
544 Syakur, M. A., Khotimah, B. K., Rochman, E. M. S., & Satoto, B. D. (2018). Integration K-Means
545   Clustering Method and Elbow Method For Identification of The Best Customer Profile
546   Cluster. *2nd International Conference on Vocational Education and Electrical Engineering
547   (Icvee), 336*. <Go to ISI>://WOS:000435606700017
548 Tan, J. G., Zheng, Y. F., Tang, X., Guo, C. Y., Li, L. P., Song, G. X., et al. (2010). The urban heat
549   island and its impact on heat waves and human health in Shanghai. *International Journal
550   of Biometeorology, 54*(1), 75-84. <Go to ISI>://WOS:000273746000008
551 Thirumalai, K., DiNezio, P. N., Okumura, Y., & Deser, C. (2017). Extreme temperatures in
552   Southeast Asia caused by El Nino and worsened by global warming. *Nat Commun, 8*,
553   15531. https://www.ncbi.nlm.nih.gov/pubmed/28585927
554 Thompson, D. W. J., Barnes, E. A., Deser, C., Foust, W. E., & Phillips, A. S. (2015). Quantifying the
555   Role of Internal Climate Variability in Future Climate Trends. *Journal of Climate, 28*(16),
556   6443-6456. <Go to ISI>://WOS:000359655200009
557 Thrasher, B., Maurer, E. P., McKellar, C., & Duffy, P. B. (2012). Technical Note: Bias correcting
558   climate model simulated daily temperature extremes with quantile mapping. *Hydrology
559   and Earth System Sciences, 16*(9), 3309-3314. <Go to ISI>://WOS:000310475400018
560 Vrac, M., Drobinski, P., Merlo, A., Herrmann, M., Lavaysse, C., Li, L., & Somot, S. (2012).
561   Dynamical and statistical downscaling of the French Mediterranean climate: uncertainty

562   assessment. *Natural Hazards and Earth System Sciences, 12*(9), 2769-2784. <Go to
563   ISI>://WOS:000310478300005
564 Watanabe, S., Kanae, S., Seto, S., Yeh, P. J. F., Hirabayashi, Y., & Oki, T. (2012). Intercomparison
565   of bias-correction methods for monthly temperature and precipitation simulated by
566   multiple climate models. *Journal of Geophysical Research-Atmospheres, 117*. <Go to
567   ISI>://WOS:000312408800002
568 Wobus, C., Zarakas, C., Malek, P., Sanderson, B., Crimmins, A., Kolian, M., et al. (2018).
569   Reframing Future Risks of Extreme Heat in the United States. *Earths Future, 6*(9), 1323-
570   1335. <Go to ISI>://WOS:000447388800010
571 Wood, A. W., Leung, L. R., Sridhar, V., & Lettenmaier, D. P. (2004). Hydrologic implications of
572   dynamical and statistical approaches to downscaling climate model outputs. *Climatic
573   Change, 62*(1-3), 189-216. <Go to ISI>://WOS:000188531900008
574 Wuebbles, D. J., Fahey, D. W., & Hibbard, K. A. (2017). Climate science special report: fourth
575   national climate assessment, volume I.
576 Zhang, G., Zeng, G., Li, C., & Yang, X. (2020). Impact of PDO and AMO on interdecadal variability
577   in extreme high temperatures in North China over the most recent 40-year period.
578   *Climate Dynamics, 54*(5), 3003-3020.

579

580

581
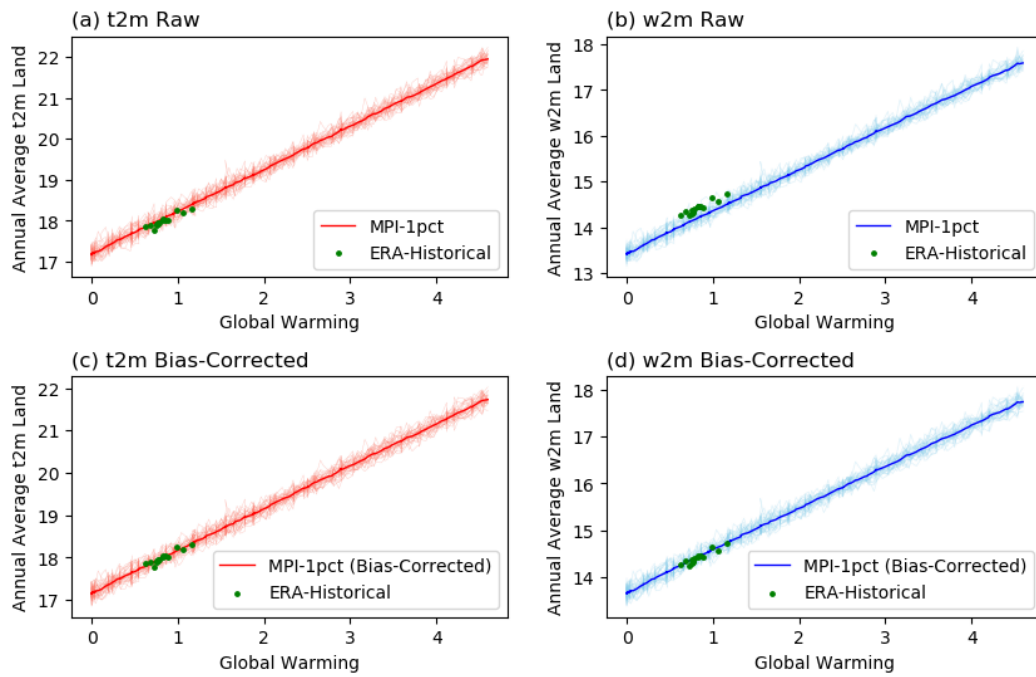
Figure 1. (a) Annual average temperature (t2m) for 150-yr 1% runs, calculated for land and

near-land ocean areas. Green dots show the historical record of ERA-Interim for the

corresponding global warming levels. (b) Same as (a), but for wet-bulb temperature (w2m). (c, d)

same as (a, b), but for the bias-corrected 1% runs.

586

587
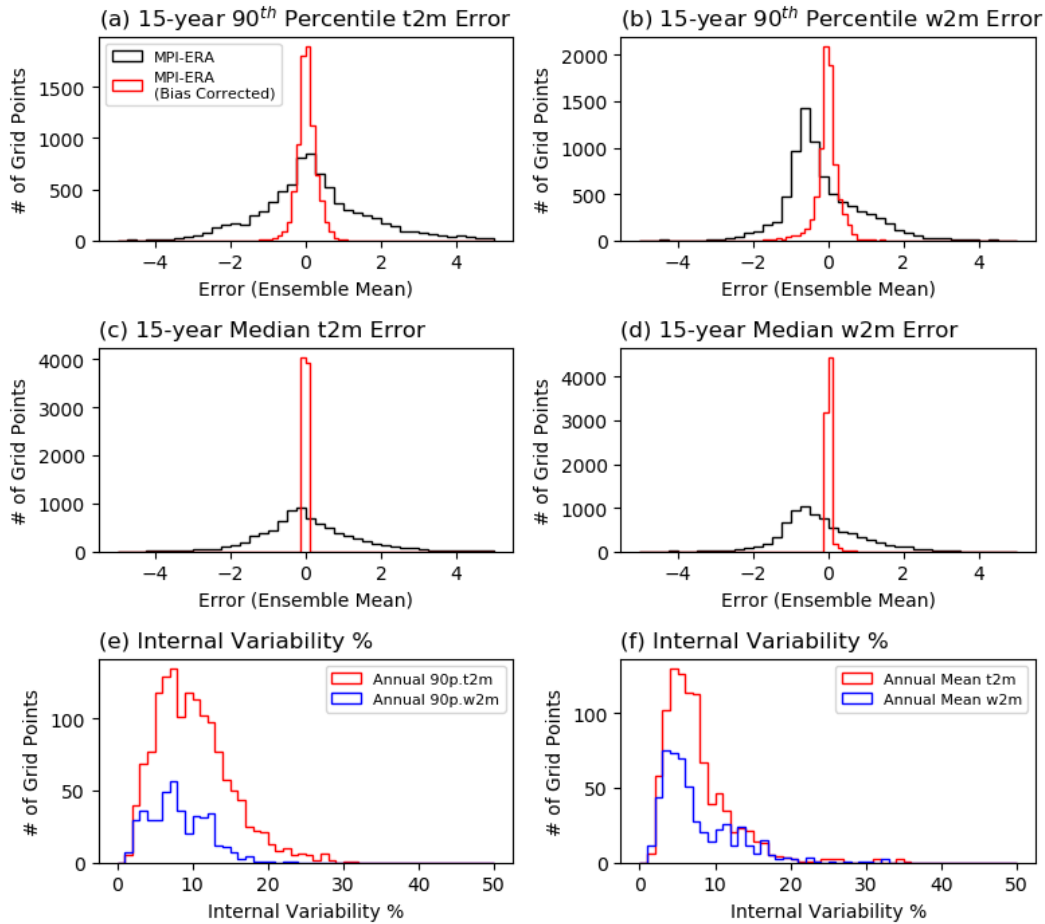
Figure 2. Histogram of (a, c) 2m temperature and (b, d) wet bulb temperature error (MPI minus

ERA) between ERA-Interim and 1% MPI runs with the same global average temperature. The

error of the (a, b) 15-year 90th percentile and (c, d) median are shown. (e, f) The percentage of

unforced variability (maximum ensemble member – minimum ensemble member) against

absolute value of the average difference with reanalysis.

594
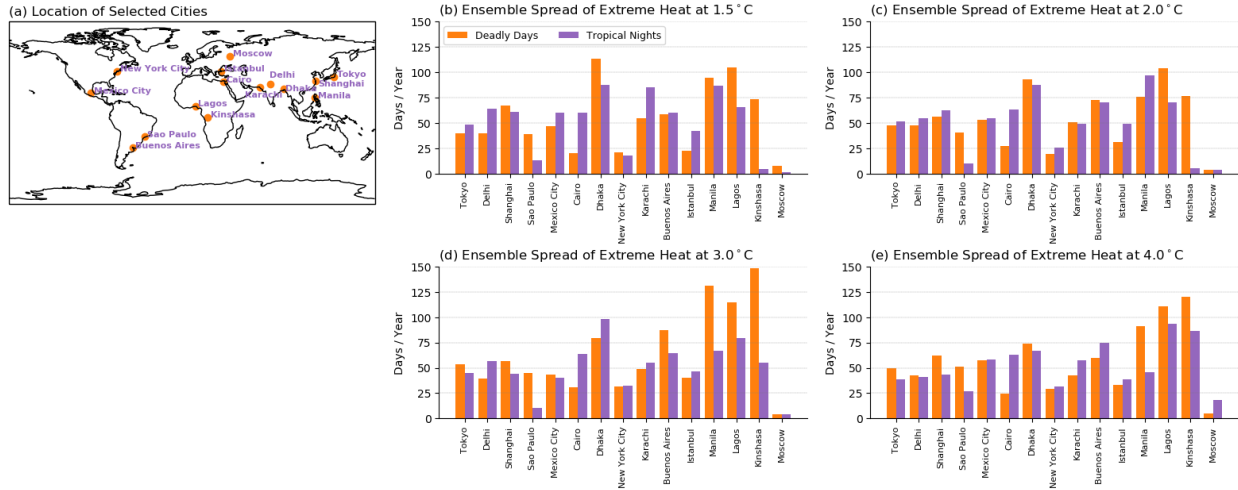
Figure 3. (a) Location of 15 selected cities and spread of heat extremes between ensemble members in (b) 1.5, (c) 2.0, (d) 3.0, and (e) 4.0°C of global warming. Ensemble with smallest heat extreme days are deducted from the ensemble with most heat extreme days to calculate the spread. Number of heat extreme days are calculated by averaging 3×3 grid covering the selected city.
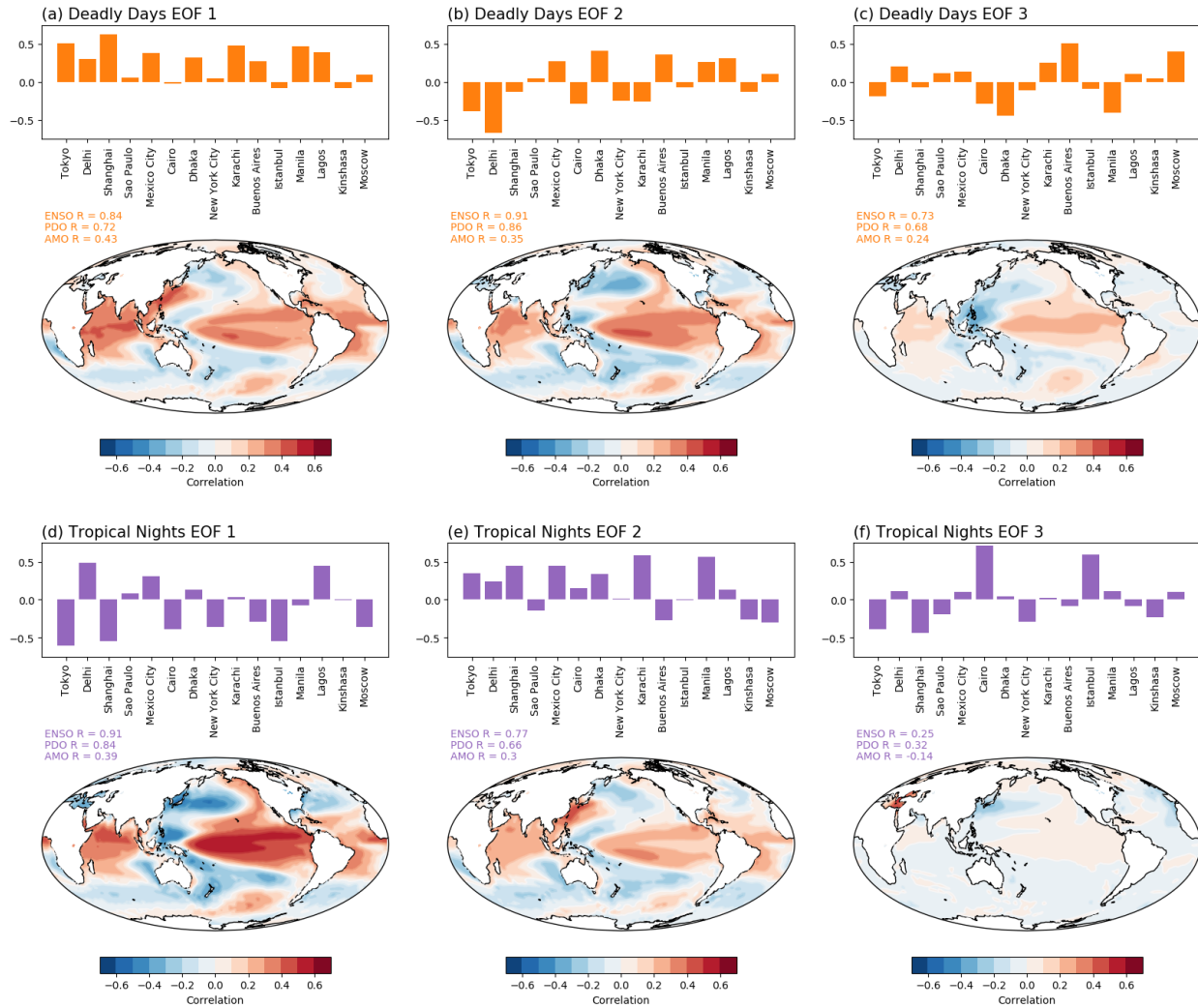
Figure 4. First three EOFs of deadly days (a, b, c) and tropical nights (d, e, f) in 15 cities. Heat extremes in 15 cities are linearly detrended and normalized before EOF analysis. For each panel, the bar graph shows the EOF pattern of the number of heat extremes days per year. Contour plots shows the SST pattern associated with the EOF mode, obtained by projecting each mode of PC onto SST anomalies. Ensemble members are averaged to yield the SST pattern. Pattern correlation with major modes of climate variability (ENSO, PDO, AMO) are also shown, as discussed in the text.

609
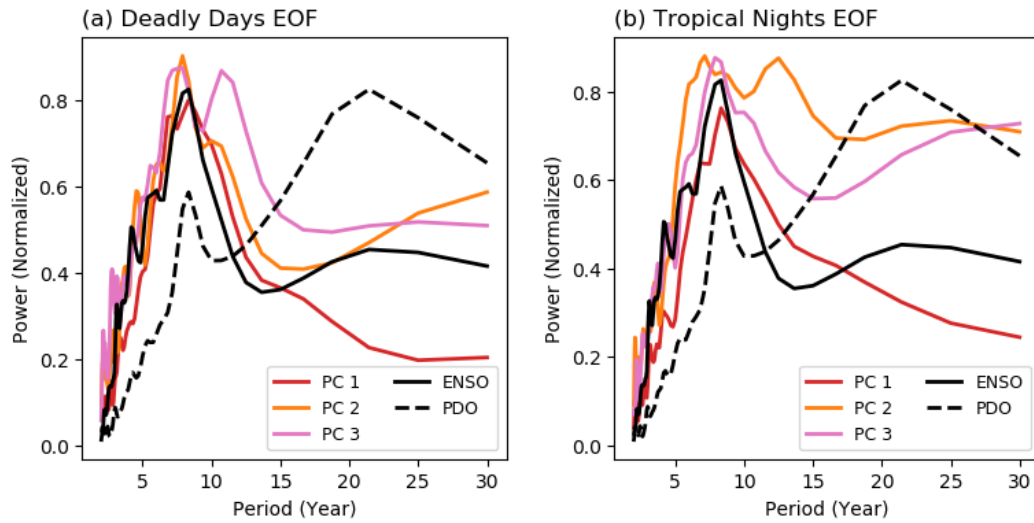
Figure 5. Frequency power spectrum of ENSO, PDO, and PC of first three EOF modes for (a)

deadly days and (b) tropical nights. ENSO is calculated with the Niño 3.4 Index, and PDO is

calculated as a leading EOF of SST anomaly in North Pacific basin. Monthly SST data is used

for both ENSO and PDO, and then each index is averaged over the year to have consistency with

deadly days and tropical nights.

615

616
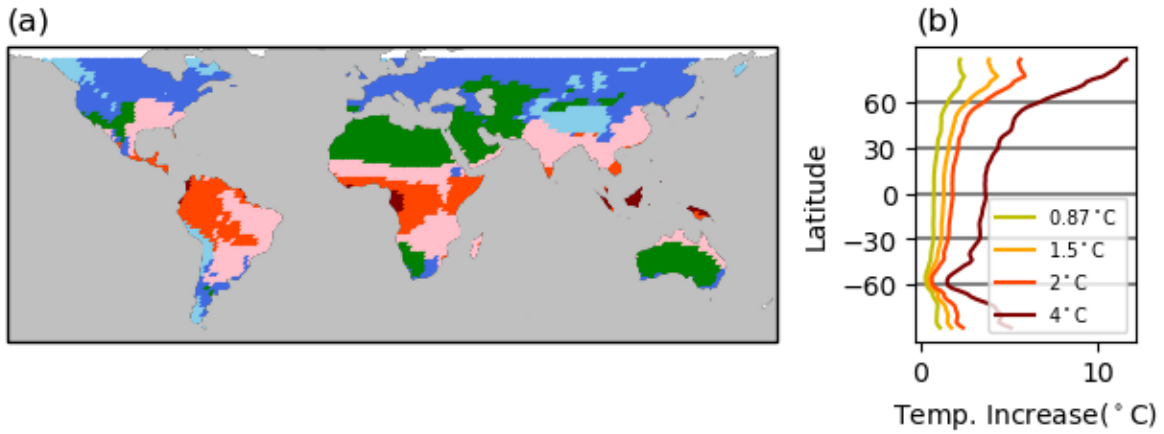
Figure 6. (a) Clustered regions via K-means clustering. (b) Zonal average of temperature

increases at the time of 0.87°C (current climate), 1.5°C, 2°C, and 4°C of global warming

compared to pre-industrial baseline in the 1% runs. Temperatures are averaged over a 5-year

period after each warming threshold is observed.

623
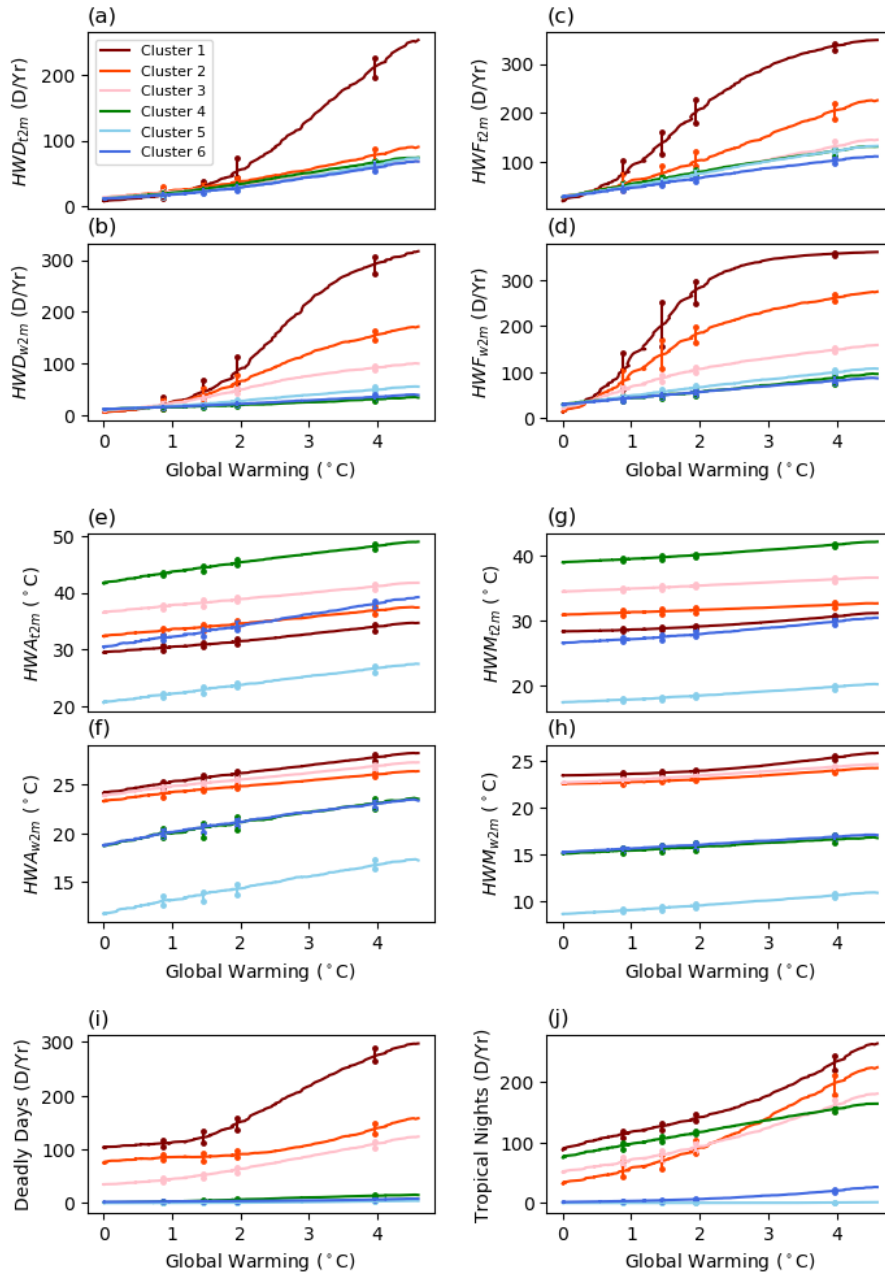
Figure 7. Evolution of each index averaged over each cluster. Values of each metric are

calculated by averaging grid points belonging to each cluster separately for each ensemble.

Vertical lines with dots show the maximum and minimum of 28 ensemble members at each

threshold of warming to represent the spread between the ensemble.

628

629
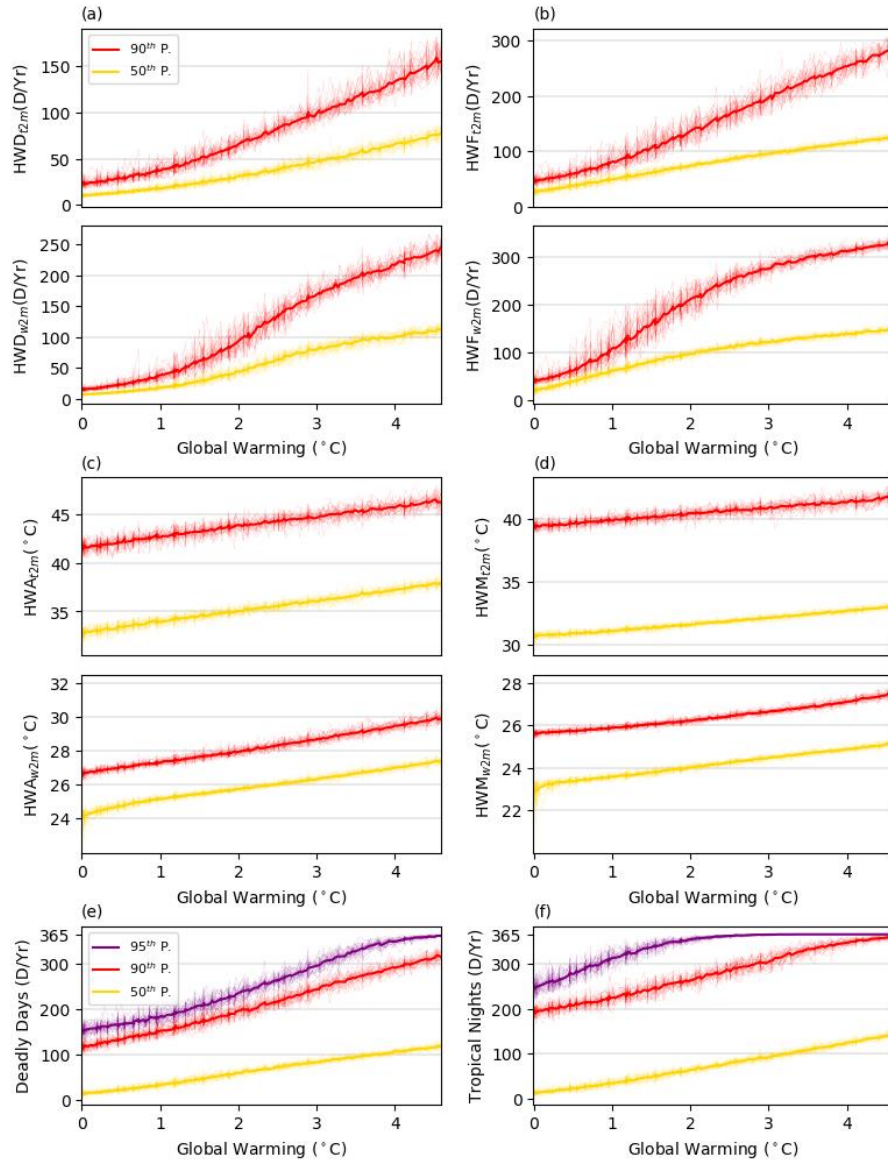
Figure 8. Changes of population-weighted heat wave indices at each level of global warming.

Each line denotes one ensemble member for percentile of population.

630

631

632

(a) Deadly Days Per Year

Warming \ GDP Percentile	0	10	20	30	40	50	60	70	80	90
3.0	279	170	246	127	108	66	71	50	105	47
2.0	230	140	203	107	91	56	58	42	83	41
1.0	173	108	147	81	69	44	45	32	58	31
0.5	144	91	120	66	59	37	40	27	48	26

(b) Tropical Nights Per Year

Warming \ GDP Percentile	0	10	20	30	40	50	60	70	80	90
3.0	338	227	290	207	137	73	82	111	70	58
2.0	277	187	234	171	117	63	68	93	61	46
1.0	219	151	182	136	93	51	56	73	51	35
0.5	197	136	162	122	83	47	51	64	46	31

Figure 9. Increase in (a) Deadly Days and (b) Tropical Nights compared to our present climate, binned by percentile of GDP per capita at selected levels of warming compared to present day, averaged over the population within the GDP percentile (for example, averaged over population in 0~10 percentile of GDP), and over all ensemble members for 5-year window after each level of warming first occurs. Blue text inside the heatmap represent the absolute of Deadly Days and Tropical Nights in each level of warming above present day.

641
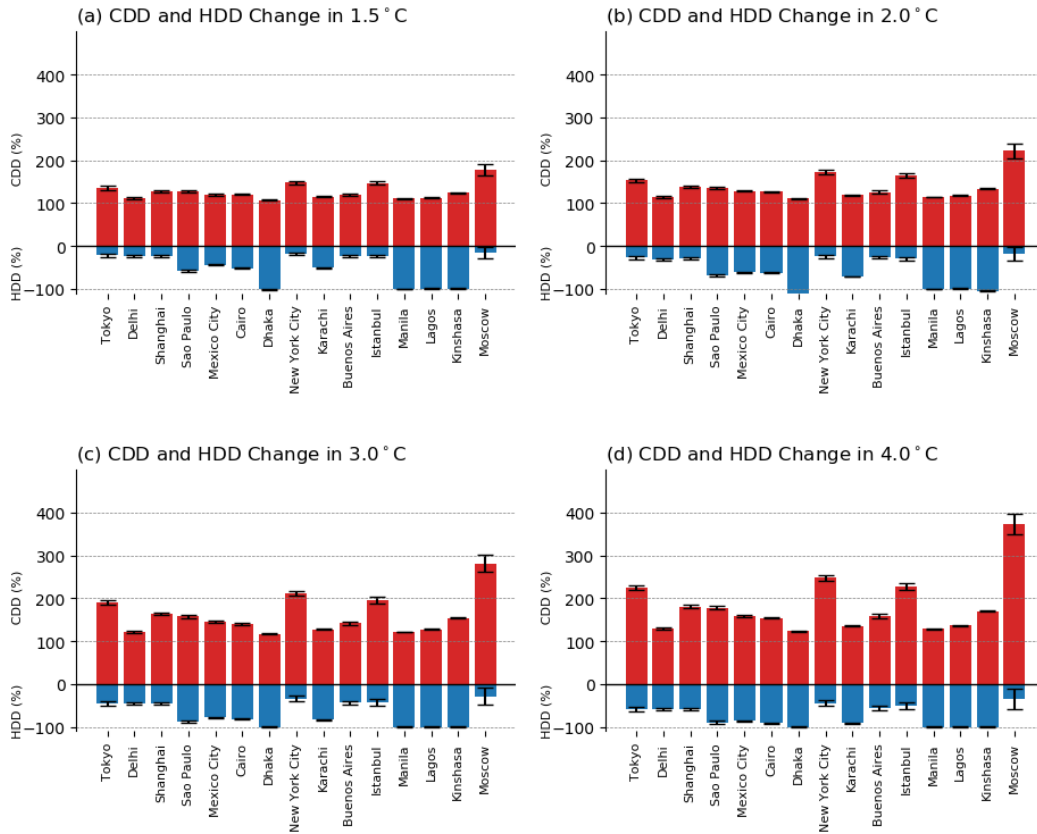
Figure 10. CDD (red bar) and HDD (blue bar) values at each levels of global warming, divided

by the pre-industrial CDD and HDD for 15 selected cities. Error bars show the standard

deviation between the ensemble members.

645

646   **Table 1.** Explanation of heat wave indices used in this study.

Acronym	Index	Definition	Units
$HWD_{t2m/w2m}$	Heat wave duration	Length of longest period of consecutive heat wave days in a year	# days
$HWF_{t2m/w2m}$	Heat wave frequency	Total number of heat wave days in a year	# days
$HWA_{t2m/w2m}$	Heat wave amplitude	Maximum temperature over all heat wave days in a year	°C
$HWM_{t2m/w2m}$	Heat wave mean	Average temperature over all heat wave days in a year	°C
Deadly Days	Deadly Days	Daily maximum wet-bulb temperature over 24°C	# days
Tropical Nights	Tropical Nights	Daily minimum temperature over 25°C	# days
CDD	Cooling degree days	Sum of positive values after removing 18°C from daily average temperature	°C days
HDD	Heating degree days	Absolute value of sum of negative values after removing 18°C from daily average temperature	°C days

647

648   **Table 2.** Percentage area and major regions belonging to each cluster. Clusters are identified

649   only for the global land areas.

Cluster	Color	Area percentage (%)	Major regions	Cluster name
1	Maroon	2.95	Indonesia, Malaysia, Cameroon, Gabon	Tropical West Pacific
2	Orange	12.34	Northern South America, Central Africa	Tropical Africa and America
3	Pink	22.70	India, Southeast Asia, Eastern South America, Southeast U.S.	Sub-Tropical Asia and America
4	Green	21.55	Northern Africa, Middle East, Australia	Deserts
5	Sky blue	7.69	Himalayas, Andes	Mountain Range
6	Blue	32.75	Canada, Northwest U.S., Russia	Sub-Polar Region

650

651 **Table 3.** Number of deadly days each percentile of global population faces with 0.87°C (current

652 period), 1.5°C, 2°C, 3°C, and 4°C global warming from the pre-industrial condition. Standard

653 deviations between the ensembles (1σ) are also shown.

	Population	Global Warming				
		0.87°C	1.5°C	2.0°C	3.0°C	4.0°C
Deadly Days	95th p.	180 ($\pm$ 13)	204 ($\pm$ 14)	228 ($\pm$ 15)	297 ($\pm$ 15)	349 ($\pm$ 6)
	90th p.	148 ($\pm$ 8)	170 ($\pm$ 9)	190 ($\pm$ 13)	244 ($\pm$ 11)	292 ($\pm$ 10)
	50th p.	31 ($\pm$ 3)	44 ($\pm$ 6)	58 ($\pm$ 5)	84 ($\pm$ 4)	105 ($\pm$ 4)
Tropical Nights	95th p.	302 ($\pm$ 14)	333 ($\pm$ 9)	350 ($\pm$ 4)	364 ($\pm$ 1)	365 ($\pm$ 0)
	90th p.	217 ($\pm$ 9)	241 ($\pm$ 13)	262 ($\pm$ 10)	306 ($\pm$ 16)	345 ($\pm$ 7)
	50th p.	32 ($\pm$ 5)	47 ($\pm$ 7)	61 ($\pm$ 5)	94 ($\pm$ 6)	122 ($\pm$ 5)

654

Figure 1.
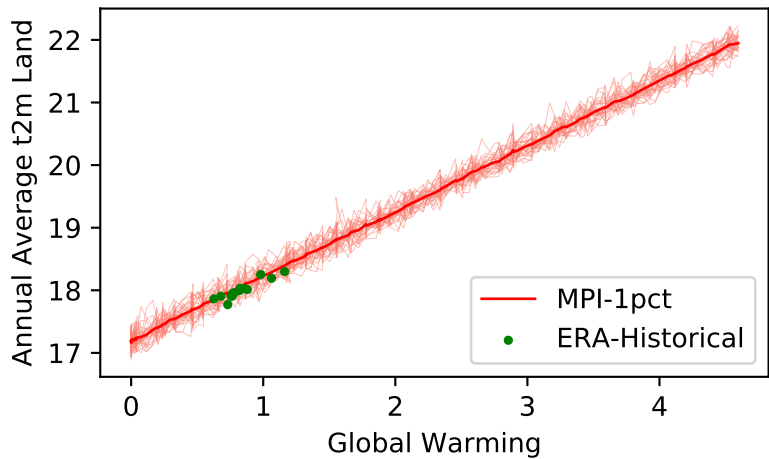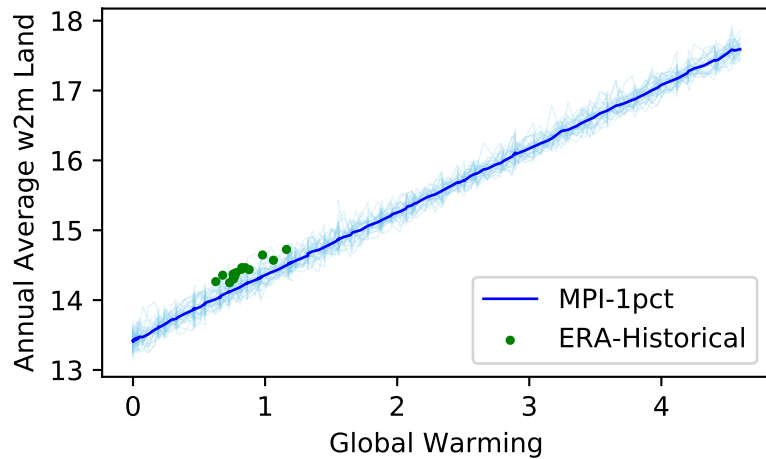
(a) t2m Raw (b) w2m Raw (c) t2m Bias-Corrected (d) w2m Bias-Corrected
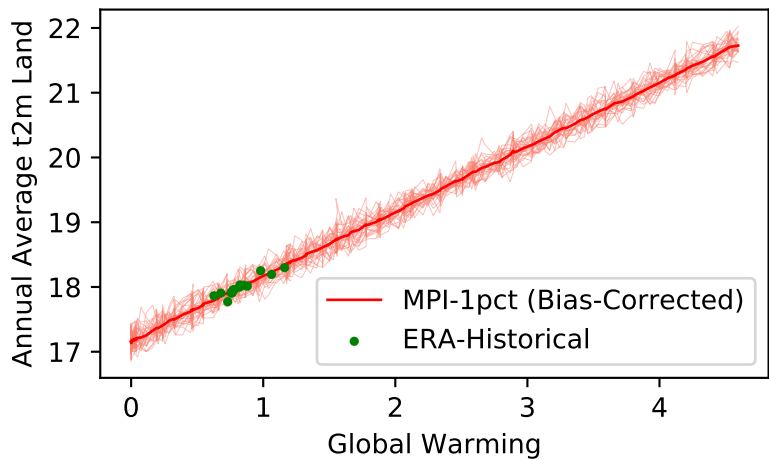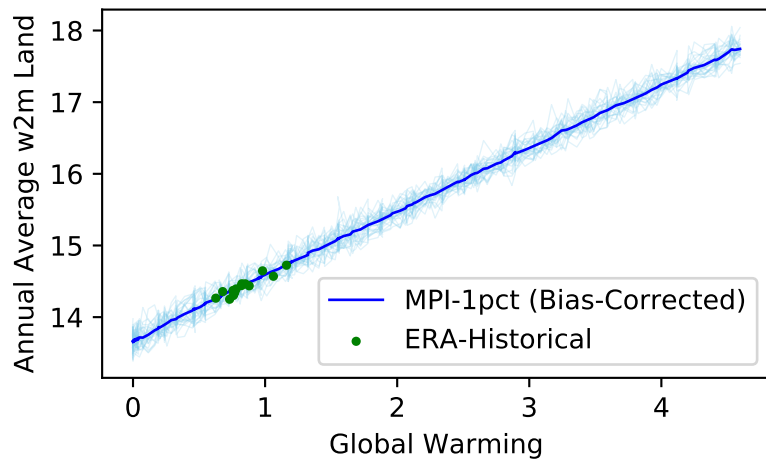
Figure 2.

(a) Annual 90th Percentile t2m Error
(b) Annual 90th Percentile w2m Error
(c) Annual Median t2m Error
(d) Annual Median w2m Error
(e) Internal Variability %
(f) Internal Variability %
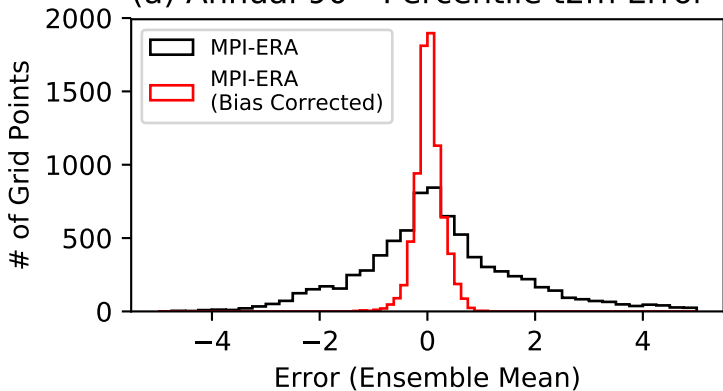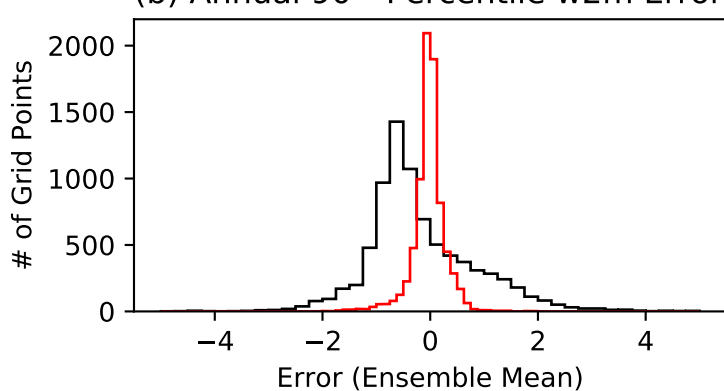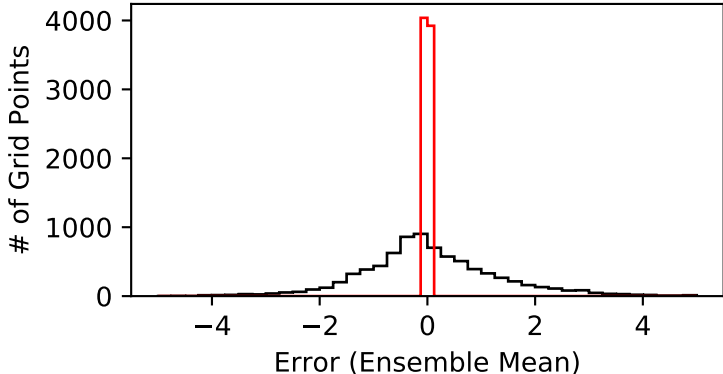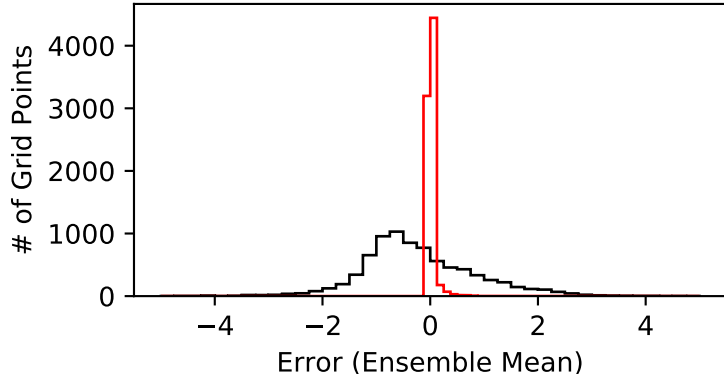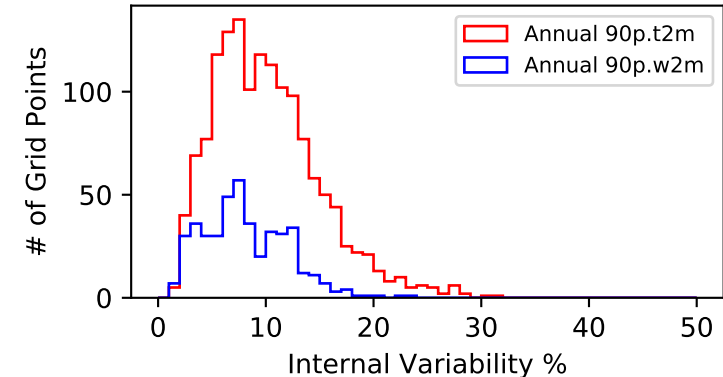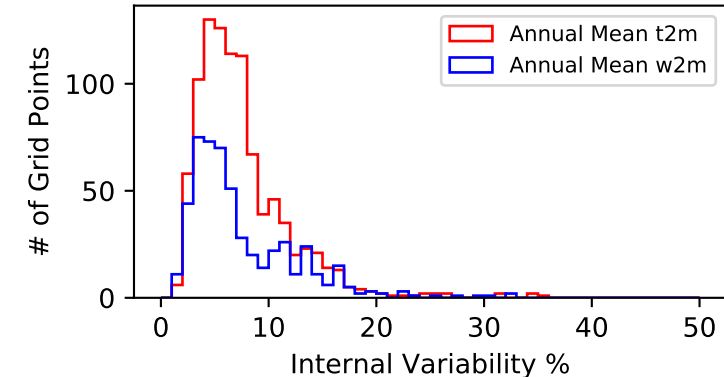
Figure 3.

(a) Location of Selected Cities
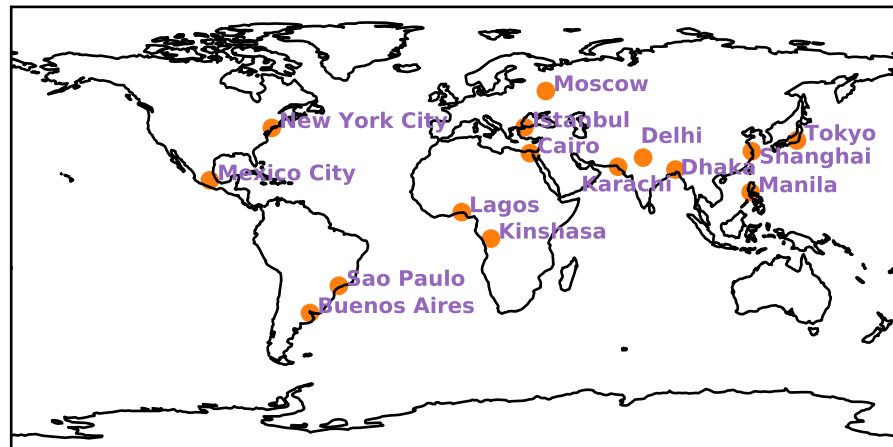
(b) Ensemble Spread of Extreme Heat in 1.5 °C
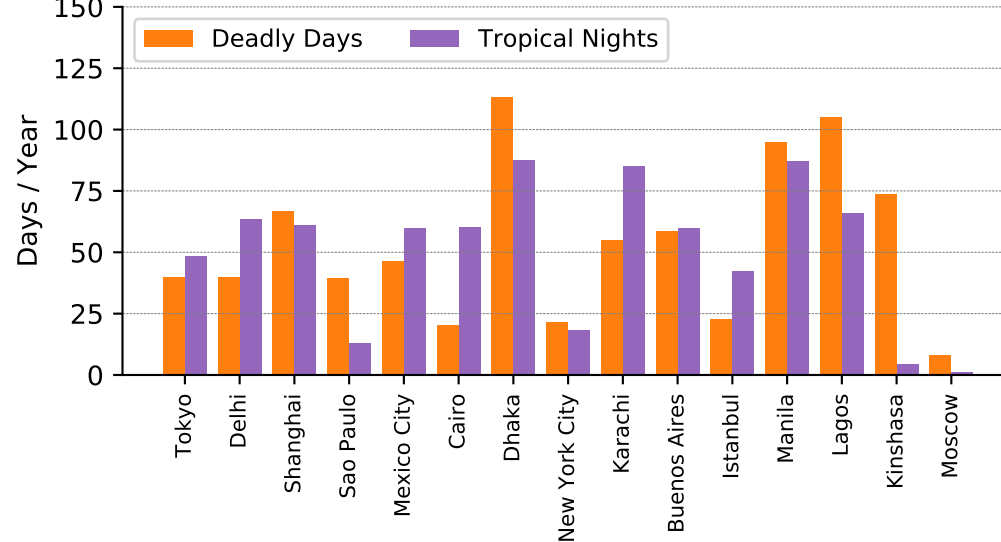
(c) Ensemble Spread of Extreme Heat in 2.0 °C
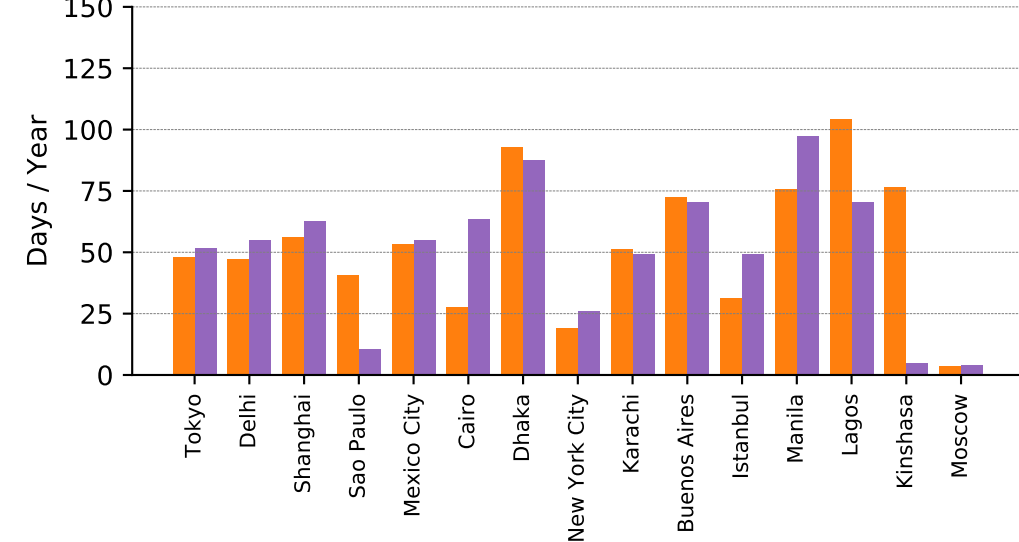
(d) Ensemble Spread of Extreme Heat in 3.0 °C
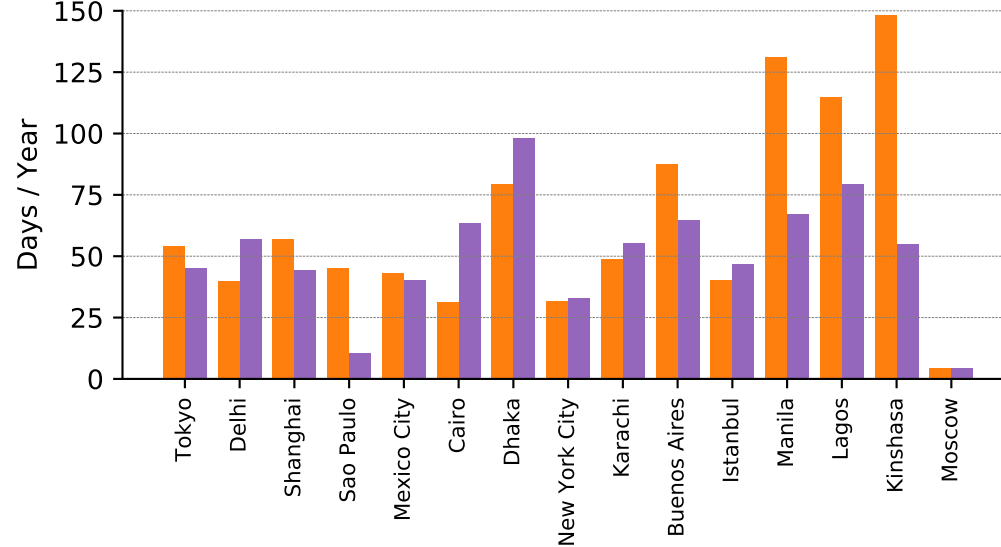
(e) Ensemble Spread of Extreme Heat in 4.0 °C
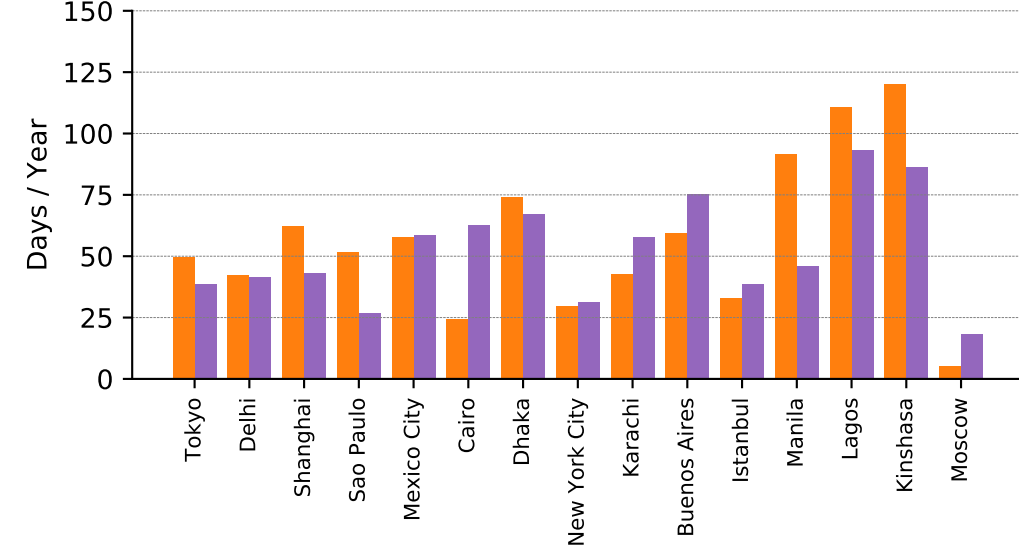
Figure 4.

(a) Deadly Days EOF 1
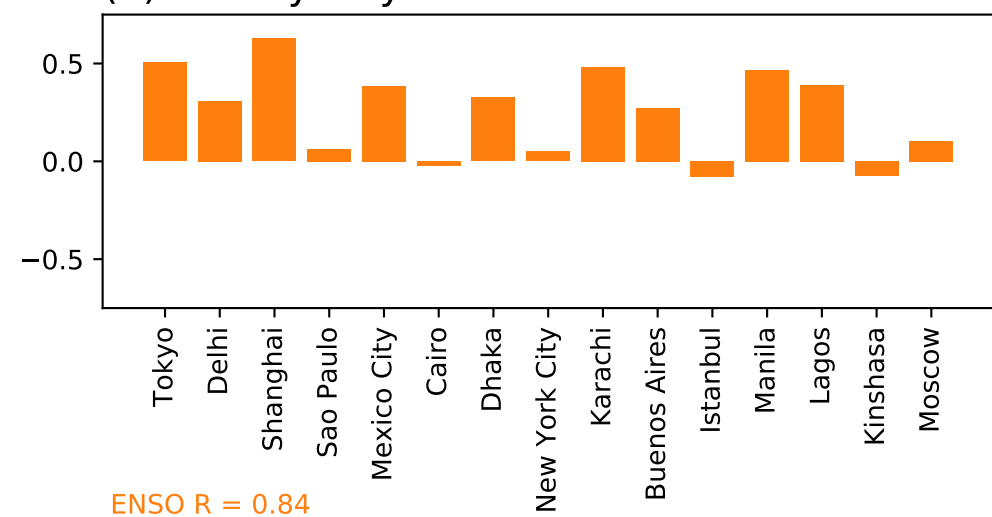
ENSO R = 0.84
PDO R = 0.72
AMO R = 0.43
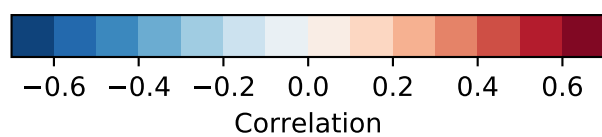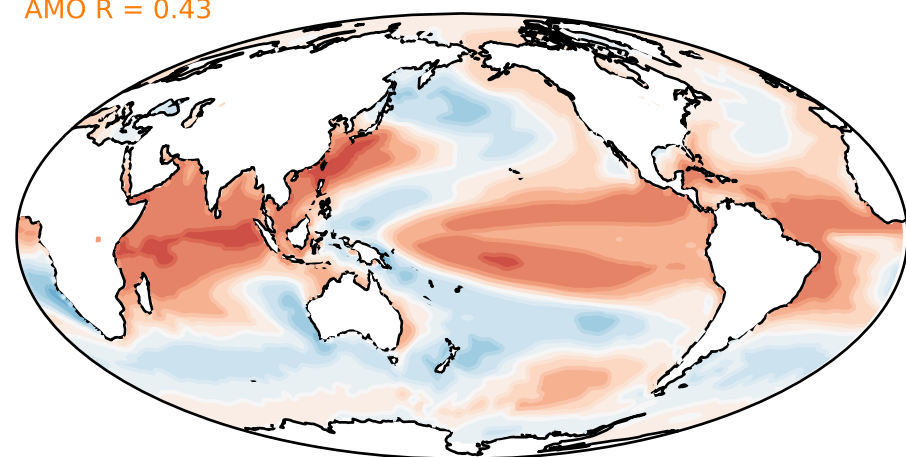
(b) Deadly Days EOF 2
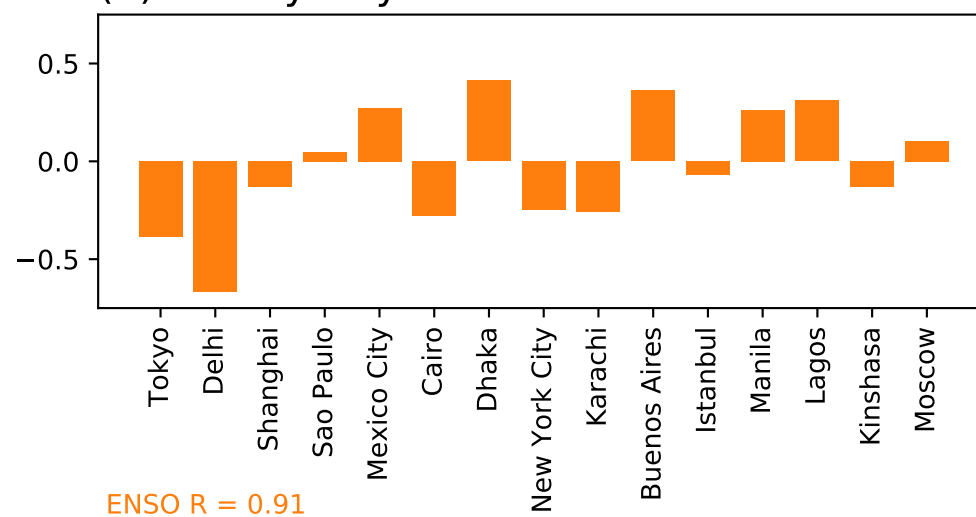
ENSO R = 0.91
PDO R = 0.86
AMO R = 0.35
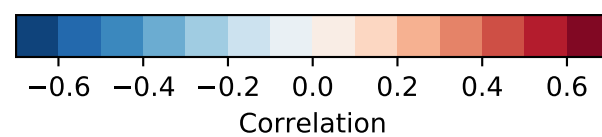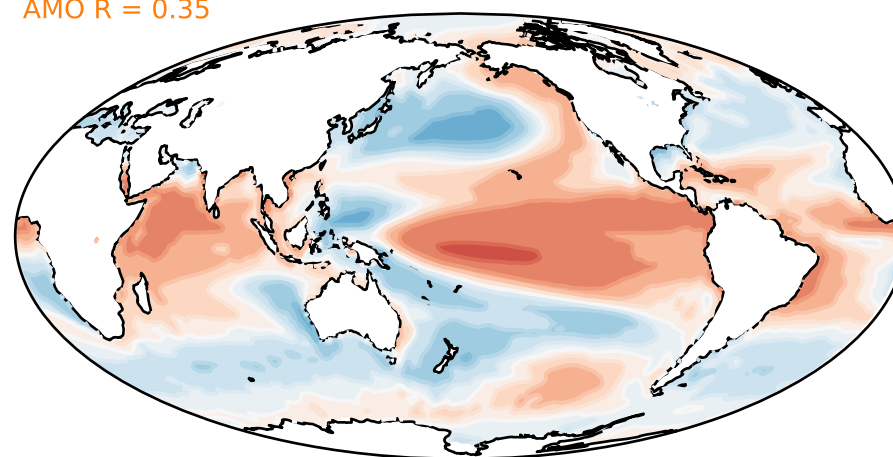
(c) Deadly Days EOF 3
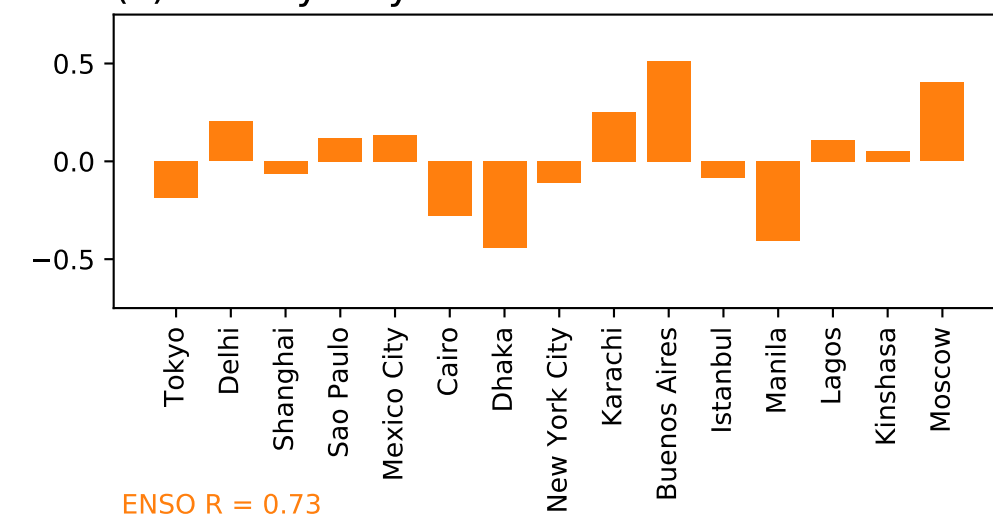
ENSO R = 0.73
PDO R = 0.68
AMO R = 0.24
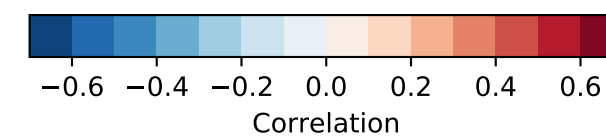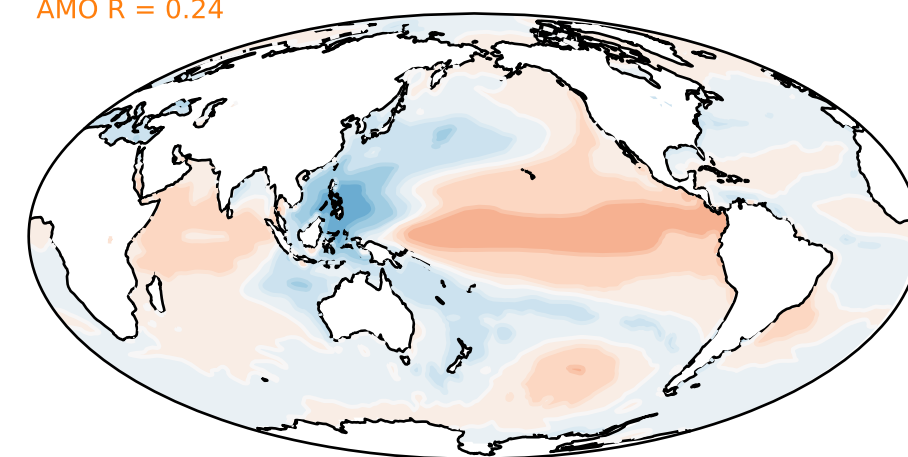
(d) Tropical Nights EOF 1
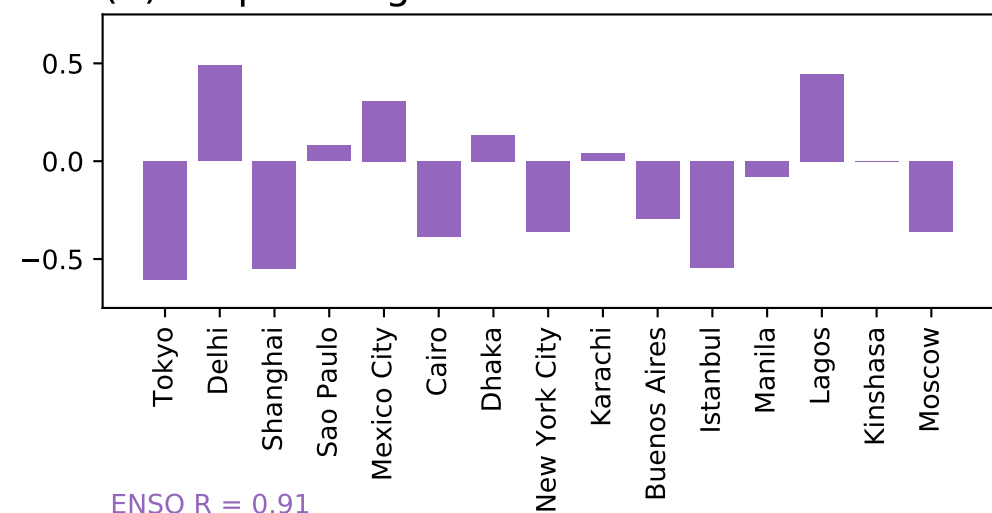
ENSO R = 0.91
PDO R = 0.84
AMO R = 0.39
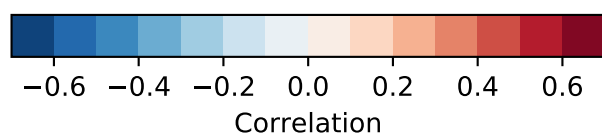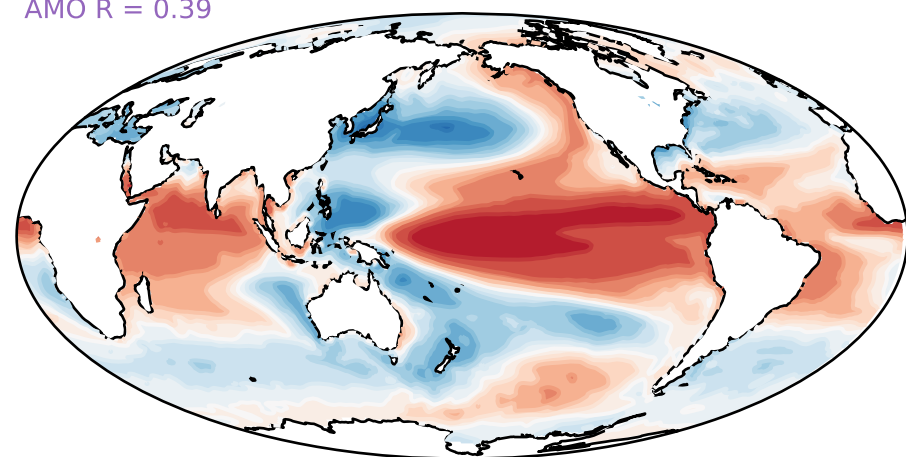
(e) Tropical Nights EOF 2
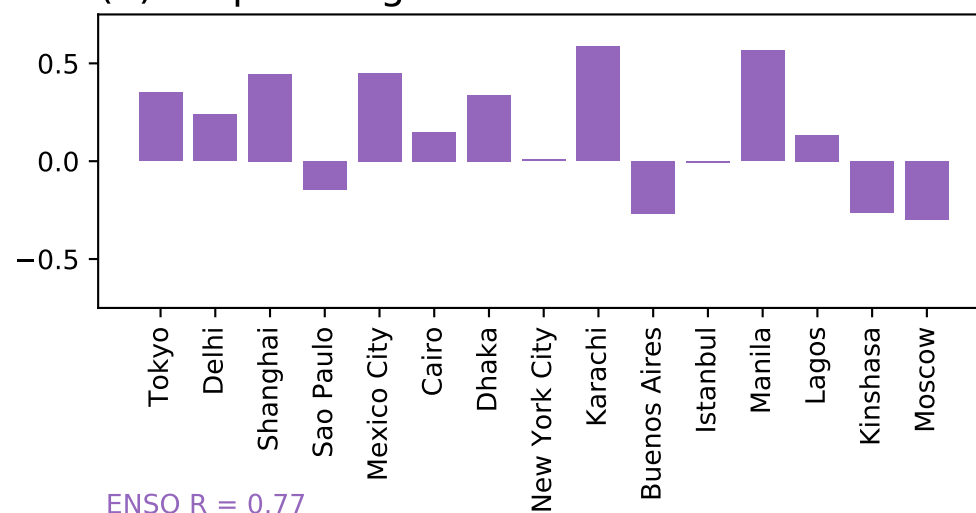
ENSO R = 0.77
PDO R = 0.66
AMO R = 0.3
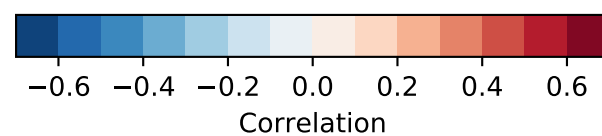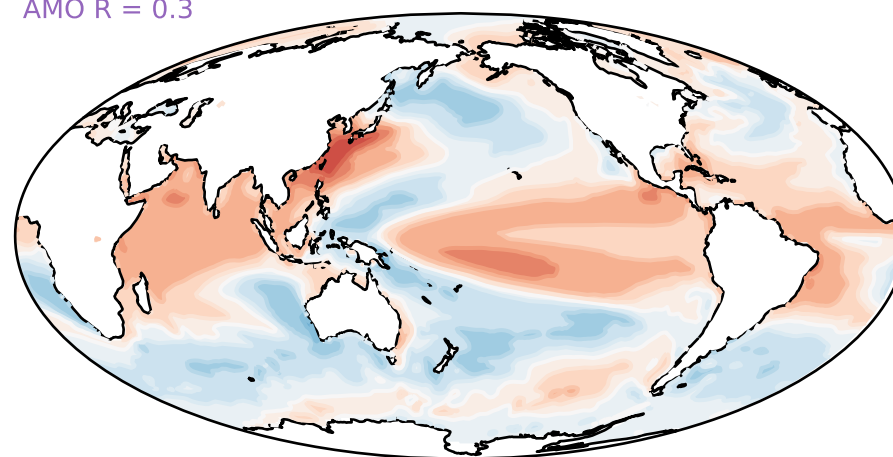
(f) Tropical Nights EOF 3
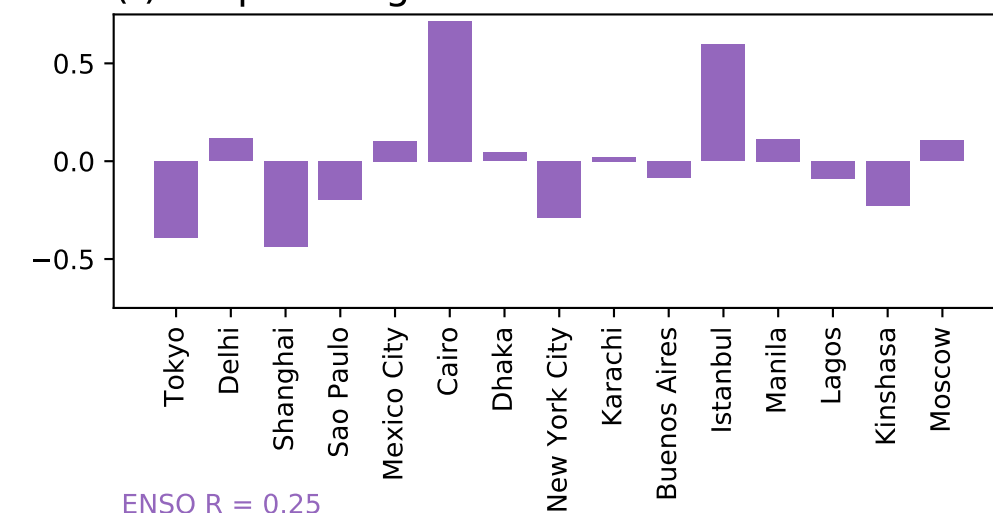
ENSO R = 0.25
PDO R = 0.32
AMO R = -0.14

Figure 5.

Figure: (a) Deadly Days EOF and (b) Tropical Nights EOF. Power (Normalized) versus Period (Year) for PC 1, PC 2, PC 3, ENSO, and PDO.

Figure 6.

(a)

(b)

| Temp. Increase (°C) |
| 0.87 °C |
| 1.5 °C |
| 2 °C |
| 4 °C |
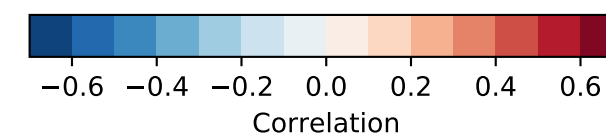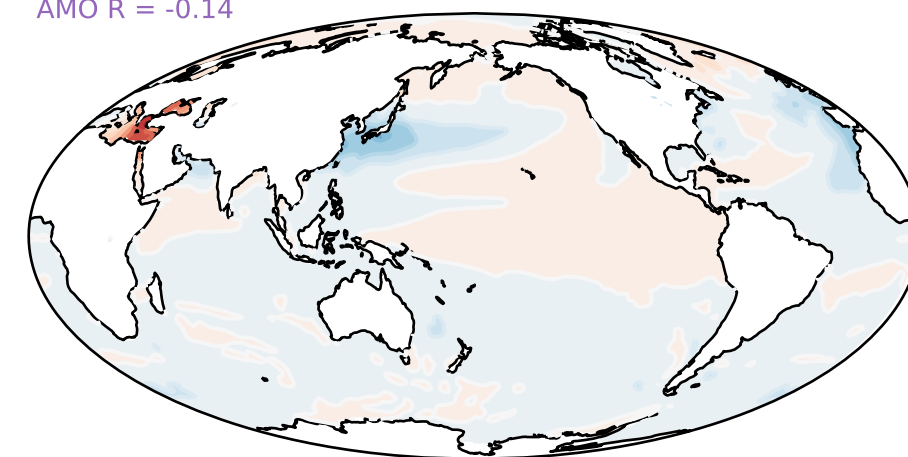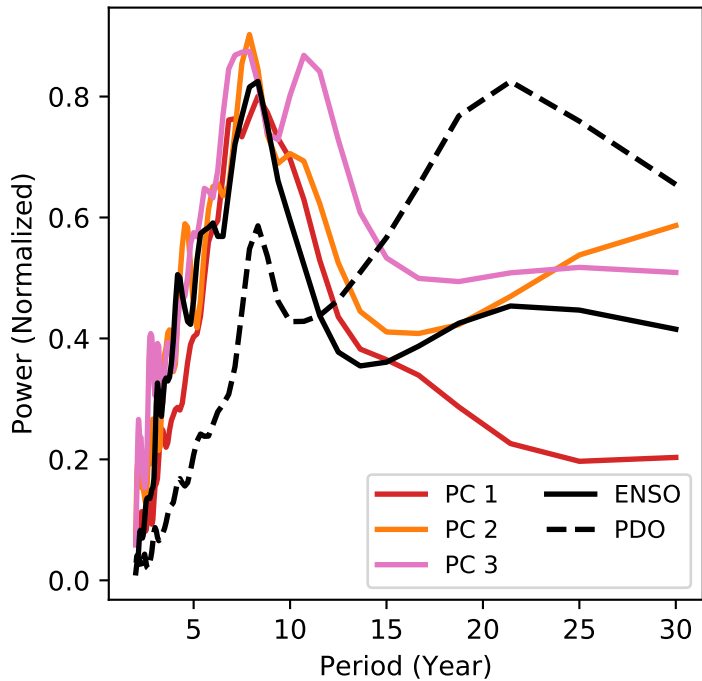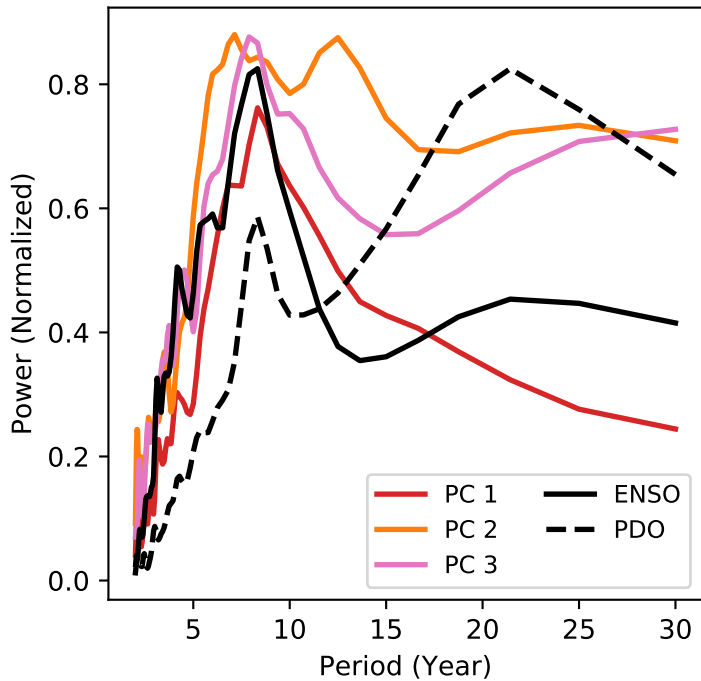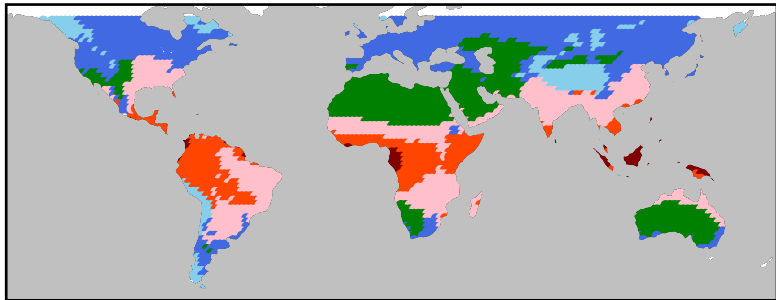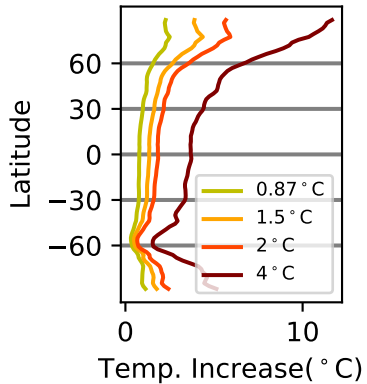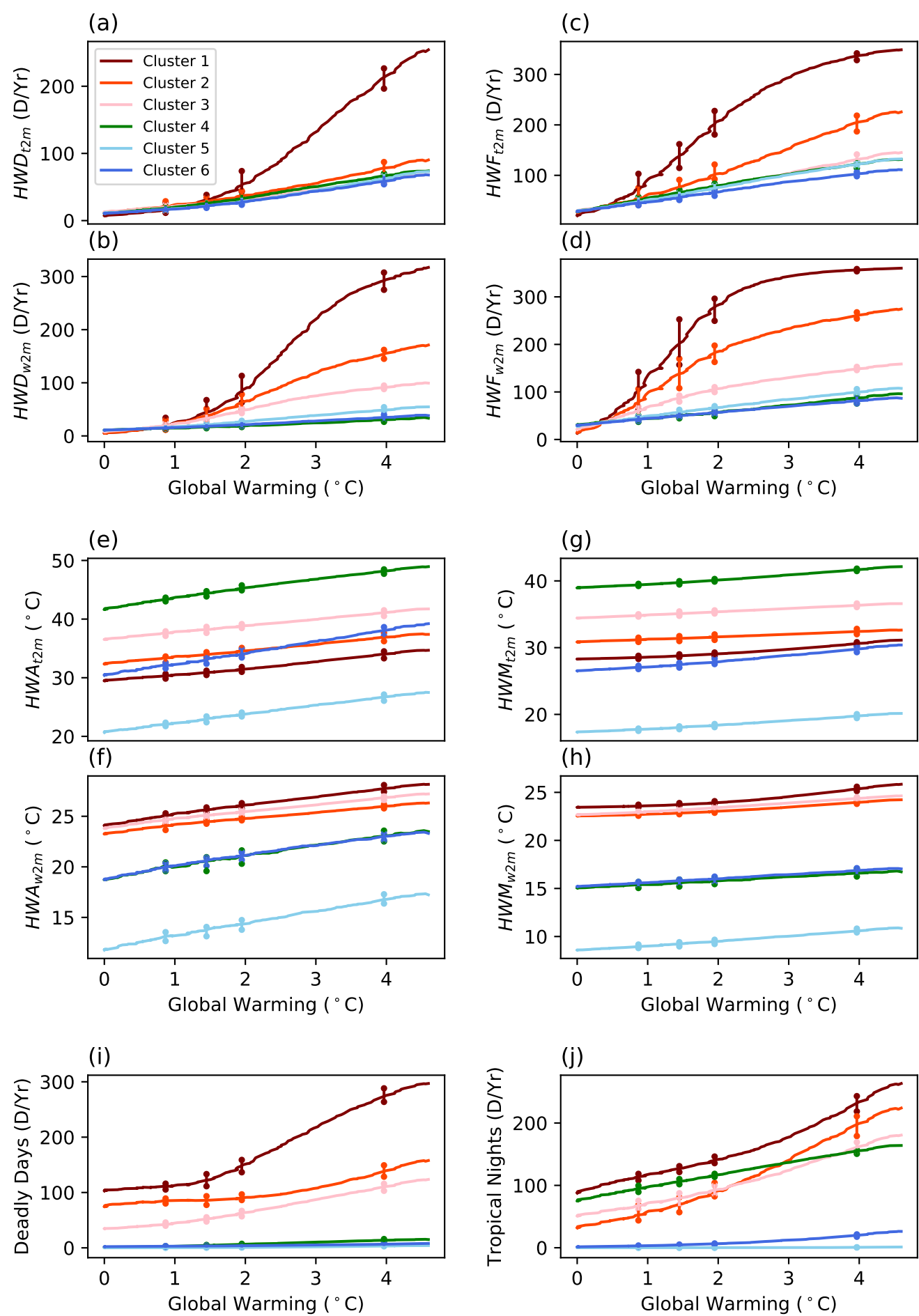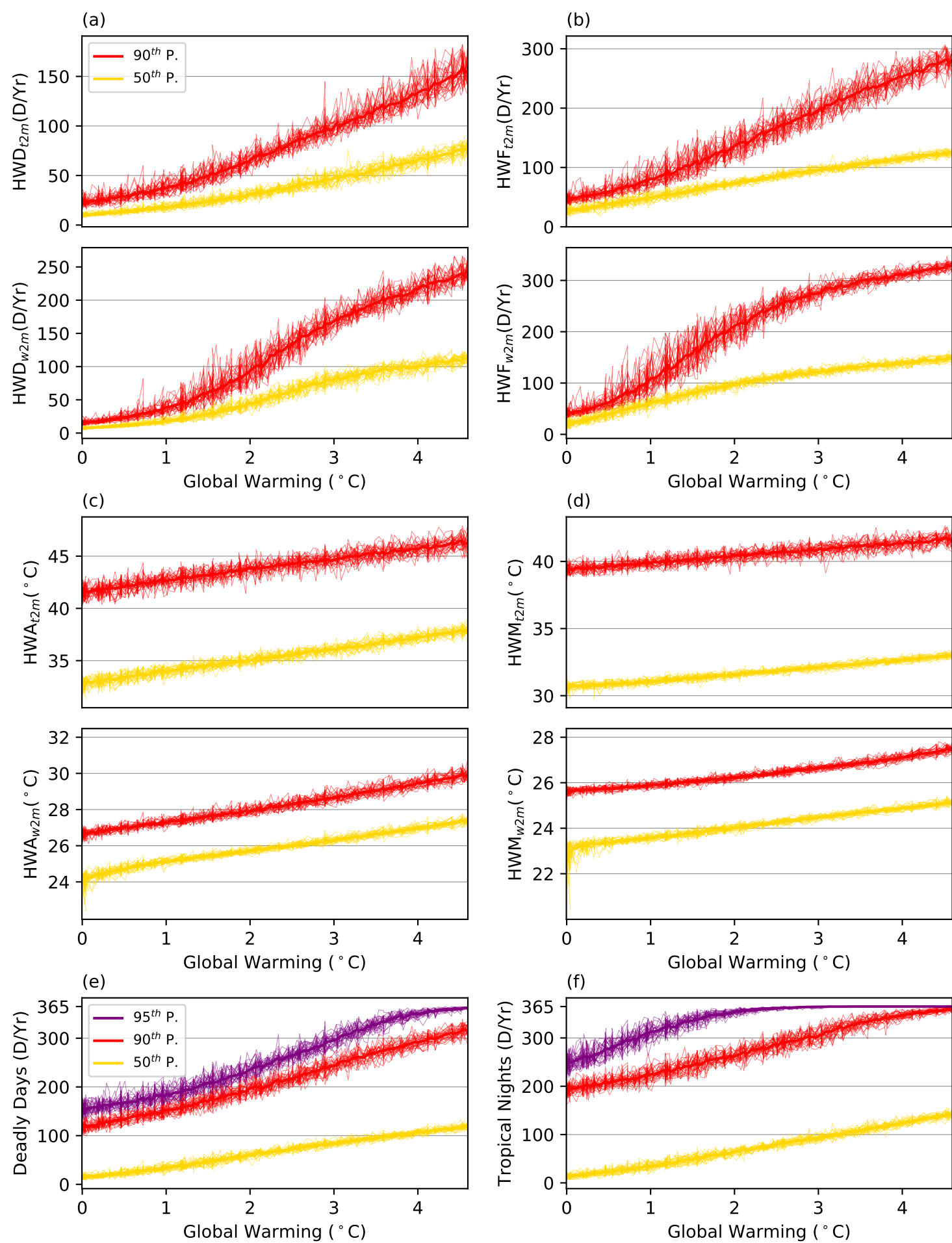
Figure 7.

Figure 8.

Figure 9.

(a) Deadly Days Per Year

Warming from present day (°C) \ GDP Percentile	0–10	10–20	20–30	30–40	40–50	50–60	60–70	70–80	80–90	90–100
3.0	279	170	246	127	108	66	71	50	105	47
2.0	230	140	203	107	91	56	58	42	83	41
1.0	173	108	147	81	69	44	45	32	58	31
0.5	144	91	120	66	59	37	40	27	48	26

(b) Tropical Nights Per Year

| Warming from present day (°C) \ GDP Percentile	0–10	10–20	20–30	30–40	40–50	50–60	60–70	70–80	80–90	90–100
3.0	338	227	290	207	137	73	82	111	70	58
2.0	277	187	234	171	117	63	68	93	61	46
1.0	219	151	182	136	93	51	56	73	51	35
0.5	197	136	162	122	83	47	51	64	46	31

Figure 10.
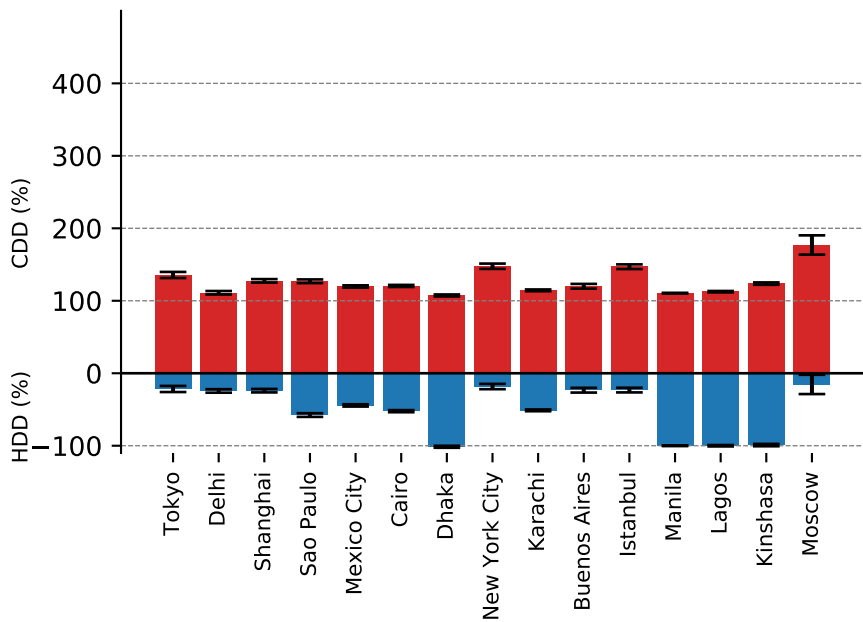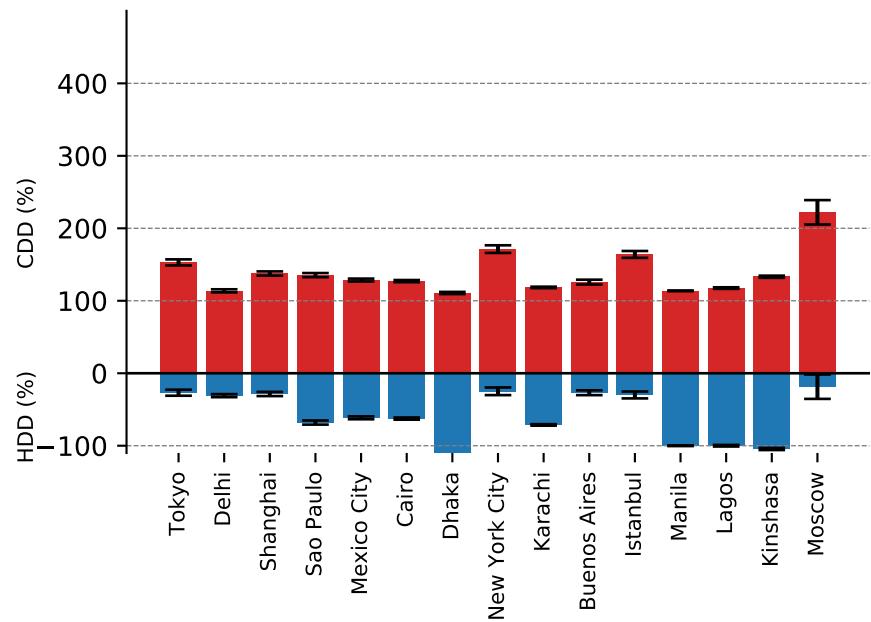
(a) CDD and HDD Change in 1.5 °C
(b) CDD and HDD Change in 2.0 °C
(c) CDD and HDD Change in 3.0 °C
(d) CDD and HDD Change in 4.0 °C